von Rad, U., Haq, B. U., et al., 1992
Proceedings of the Ocean Drilling Program, Scientific Results, Vol. 122

15. GEOCHEMISTRY OF PORE WATER AND SEDIMENTS RECOVERED FROM THE EXMOUTH PLATEAU[1]

Eric H. De Carlo[2]

ABSTRACT

During Leg 122, a transect was drilled across the Wombat Plateau, a marginal spur of the Exmouth Plateau, complemented by two sites on the Exmouth Plateau proper. In this report, pore-water analyses for major seawater constituents, alkalinity, Ba, Fe, Mn, Li, Sr, Rb, and silica are presented. Large gradients in the pore-water profiles provide evidence of complex sediment/pore-water interactions associated with carbonate and silica diagenesis and the formation of authigenic minerals. Diffusion affects pore-water profiles but differs considerably from site to site. Advection of freshwater, probably of continental origin, helps maintain negative Cl and salinity gradients deep within the sediments of the Exmouth Plateau.

INTRODUCTION

Six sites in passive continental margin sediments of the Exmouth and Wombat plateaus, northwest Australia, were drilled during Ocean Drilling Program (ODP) Leg 122 (Fig. 1). Pore water was sampled in Carnian to Quaternary age sediments comprised of continental and shallow marine clastics, shallow and deep marine carbonates, and authigenic minerals. To the best of my knowledge Leg 122 is the first deep ocean drilling leg to have sampled pore waters from Triassic sediments in the Southern Hemisphere.

The Exmouth Plateau is a deeply subsided fragment of rifted continental crust. The plateau began to assume its current configuration during the Late Triassic, when rifting between northwestern Australia, India, and other portions of East Gondwana began (Exon et al., 1982). Breakup and separation of the plateau occurred during the Jurassic to Early Cretaceous and was followed by the deposition of several kilometers of marine sediments. The Wombat Plateau, located at approximately 17°S, 115°E (Fig. 1), is a marginal spur of the Exmouth. A detailed description of the regional geology and tectonic evolution of the Exmouth and Wombat plateaus is given by Haq, von Rad, O'Connell, et al. (1990) and von Rad et al. (this volume).

Shipboard pore-water analyses of salinity, pH, alkalinity, Ca, Cl, Mg, sulfate, and silica concentrations, and shore-based determinations of Li, Na, K, Rb, Sr, Ba, Mn, and Fe concentrations in pore water, as well as the concentrations of Li, Na, K, Mg, Ca, Sr, Ba, Al, Si, Ti, Fe, and Mn in the sediment, are presented. Pore-water profiles are discussed in terms of sediment diagenesis and in relation to the lithology of the associated sediments.

Elemental compositions of the sediments are not strongly affected by diagenesis. Changes in elemental abundances in the bulk sediment are primarily related to changes in the dominant mineralogy of the sediments and are indicative of changes in the depositional setting of the Exmouth and Wombat plateaus over geologic time. Changes in pore-water elemental abundances, on the other hand, reflect diagenetic processes.

METHODS

Pore Water

Interstitial water was obtained by shipboard squeezing of whole-round (5–10 cm) cores at room temperature with a stainless steel press (Manheim and Sayles, 1974); samples were then filtered and stored for subsequent analyses. Alkalinity, pH, and salinity were determined immediately after sample collection. An *in-situ* harpoon (Barnes) water sampler with a temperature probe was deployed five times. Methods employed at sea have been described by Gieskes (1974) and Gieskes and Peretsman (1986) as well as in the "Explanatory Notes" chapter of the *Initial Reports* (Haq, von Rad, O'Connell, et al., 1990). Standards calibrated against or prepared from International Association of Physical Scientists Organizations (IAPSO) were used in all shipboard determinations. Acidified splits of samples in glass vials were analyzed by flame atomic absorption-emission (K, Li), furnace atomic absorption (Rb), and inductively coupled plasma atomic emission (Ba, Fe, Mn, Sr) spectrometries. Selected acidified (alkalinity) splits stored in plastic were also analyzed for Ba and compared to the glass vial split analyses; this was necessary because erroneously high Ba concentrations have been observed in samples stored in borosilicate glass (M. Mottl, pers. comm., 1989). Commercial spectroscopic standards were used for calibration and IAPSO seawater used as a check solution in all shore-based determinations. Sodium was determined by charge balance.

Sediments

Portions of the whole-round squeeze cakes and other solid samples of special interest were rinsed with distilled deionized water to remove sea salts. The sediments were freeze-dried and ground to pass 100-μm mesh standard sieves prior to further treatment. Bulk mineralogy was determined by X-ray diffractometry prior to elemental analysis. Results of the mineralogical analyses are presented elsewhere by Wilkens et al. (this volume).

Splits of all samples were dried at 110°C and dissolved in microwave digestion vessels. Carbonate-rich sediments were solubilized with HCl, whereas those containing significant amounts of aluminosilicates required a mixture of HCl, HF, and HNO_3. The microwave techniques employed in this work

---

[1] von Rad, U., Haq, B. U., et al., 1992. *Proc. ODP, Sci. Results,* 122: College Station, TX (Ocean Drilling Program).

[2] Department of Oceanography, School of Ocean and Earth Sciences and Technology, 1000 Pope Rd., University of Hawaii, Honolulu, Hawaii 96822 U.S.A.

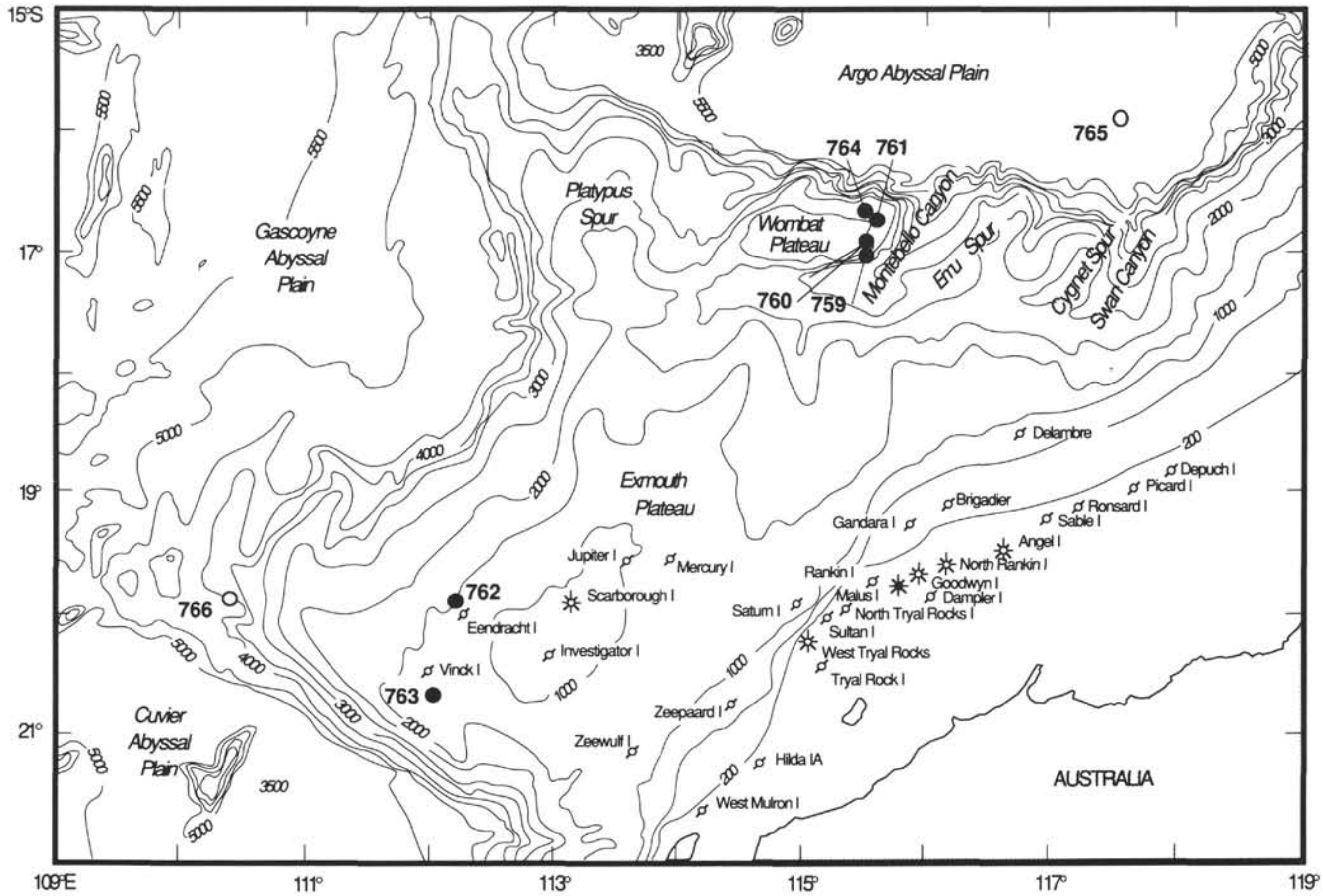

Figure 1. Area location map of the Exmouth Plateau, northwest Australia (after Haq, von Rad, O'Connell, et al., 1989).

are modifications of previously described methods (Kingston and Jassie, 1988; De Carlo, 1990). The accuracy of spectroscopic determinations was verified by the analysis of standard geological materials.

RESULTS

Wombat Plateau Sites

Variations in pore-water constituents with depth for Sites 759 through 761 are shown in Figure 2. Data from Site 764 are not presented, as only two pore-water samples were recovered at this site. A summary compilation of pore-water data for Leg 122 sites is presented in Table 1. Results of the bulk elemental analyses of sediments are presented in Table 2. These data are primarily presented to complement the mineralogical analyses given by Wilkens et al. (this volume). The composition of the sediments will be discussed only in terms of its effect on the pore-water composition.

Major-element concentrations generally exhibit greater variability with increasing depth downhole at Sites 759 and 760 than at Site 761. Similar trends are also observed for other pore-water constituents with the notable exception of Fe, Mn, and silica. The concentrations of Mg, K, and sulfate generally decrease in a regular fashion downhole (Fig. 2) to approximately 20% of the seawater value at depth. Strontium and Ba concentrations display an opposite behavior and increase downhole. The Ca profile, unlike those of most major pore-water constituents, is rather monotonous at Sites 759 and 761, but concentrations increase by nearly a factor of two in the first 200 meters below seafloor (mbsf) at Site 760. Dissolved Rb concentrations generally decrease downhole, although the data show significant scatter at Site 760. The Rb profiles appear similar to those of K.

Dissolved silica profiles are more complex than those of the major pore-water constituents. Typically, a large initial increase above the seawater concentration occurs just below the mudline (Fig. 2) that is followed by a sharp negative gradient between approximately 20 and 50 mbsf. Below this depth dissolved silica concentrations exhibit considerable scatter; large variations are observed primarily at Site 761.

Dissolved Fe increases sharply in the first 25 m of the sediment then decreases to 1–2 μmol/L at 100 mbsf. Between 100 and 150 mbsf significant increases in dissolved Fe are observed at Sites 759 and 760, whereas only a small increase occurs at Site 761. Elevated dissolved Mn concentrations immediately below the sediment/seawater interface decrease to less than 2 μmol/L by 25 mbsf, increase to maxima between 50 and 80 mbsf, then return to lower concentrations at depth. A monotonous Mn profile is observed only at Site 759.

Sites 762 and 763

Unlike the sedimentary sequences encountered at Sites 759, 760, and 761, fairly continuous sequences comprised of Quaternary through Berriasian sediments were recovered at Sites 762 and 763 (Haq, von Rad, O'Connell, et al., 1990). Much of the sediment is carbonate-rich, but grades into clay and siliciclastic-rich sediments below 800 and 500 mbsf at the two sites, respectively. Excellent core recovery led to the collection of 34 pore-water samples at Site 762 and 41 at Site 763. The sedimentary sequences at Sites 762 and 763 are

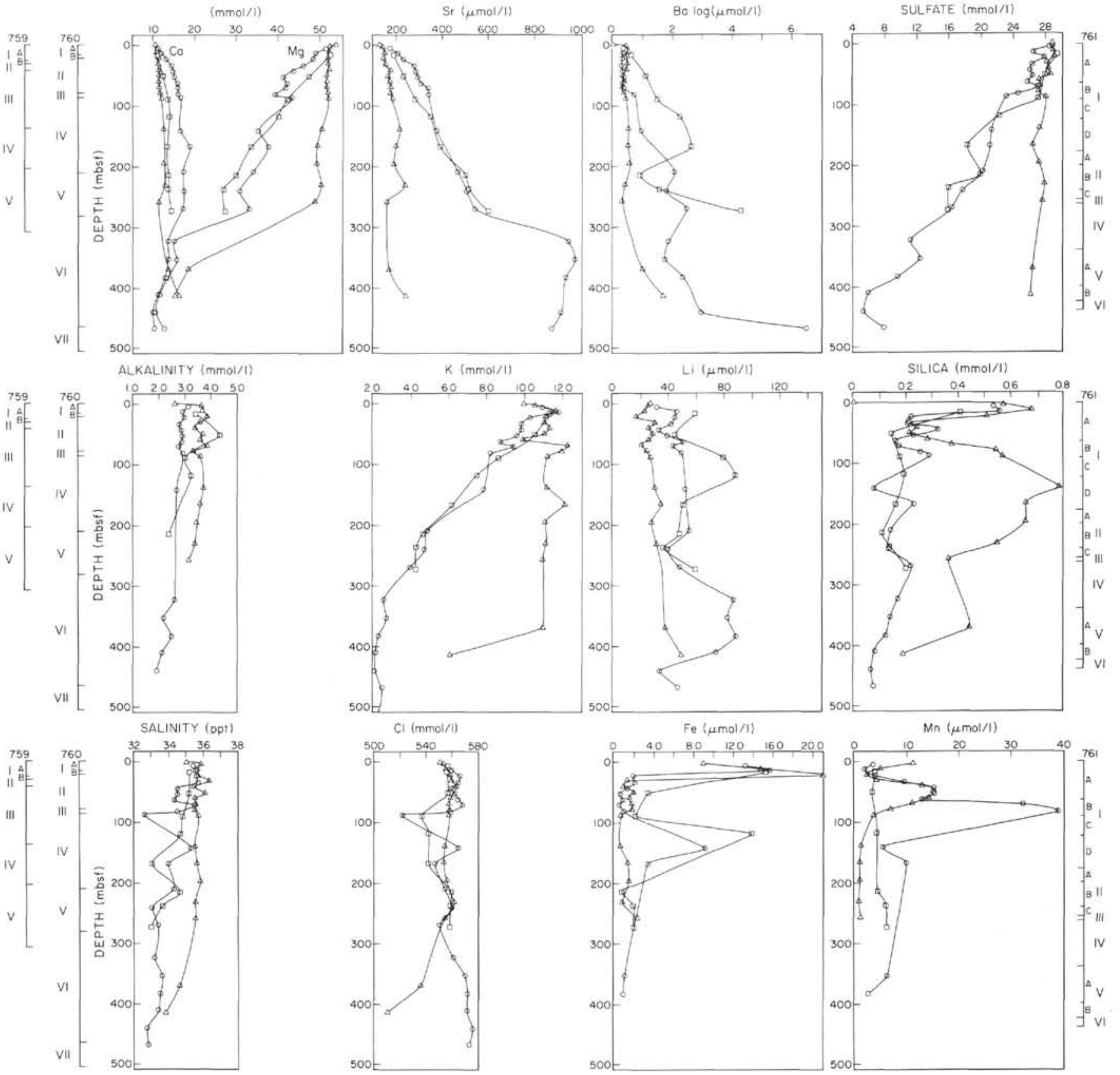

Figure 2. Wombat Plateau sites: pore-water concentrations as a function of depth with lithological units indicated to the left. Squares = Site 759, circles = Site 760, and triangles = Site 761.

similar with the exception of a major hiatus from the early Maestrichtian to middle Eocene at Site 763. Thus, the sediments from Site 763 provided the opportunity to study an expanded section of Turonian to Berriasian sediments unavailable at Site 762.

Nearly all pore-water profiles at Sites 762 and 763 (Fig. 3) are characterized by significant concentration gradients. Other differences between the Wombat Plateau sites (Fig. 2) and Sites 762 and 763 (Fig. 3) are the steeper overall dissolved Li gradient, and much steeper Sr and sulfate pore-water gradients in the uppermost sections of the latter.

Alkalinity profiles at Sites 762 and 763 are markedly different from one another. At Site 762 alkalinity gradually increases with depth for the first 370 m except for a sharp increase to 9.6 mmol/L at 404 mbsf. Below this depth, the alkalinity decreases downhole, except for a single high measurement at 887 mbsf. The alkalinity at Site 763, however, is characterized by considerable variability in the first 150 mbsf, below which a broad, well-defined maximum peaking at 320 mbsf is observed. Further downhole alkalinity fluctuates between 2 and 4 mmol/L.

Dissolved silica exhibits trends that are similar to those observed at Site 761, providing evidence of several reaction zones within the sediments. The trace element profiles are also quite variable. Dissolved Mn and Fe exhibit complex profiles at both Exmouth Plateau sites. Some similarities exist with the profiles at Site 761 (Fig. 2) and are particularly evident in the uppermost 200 m of the sediments. Three and

Table 1. Composition of pore water from Leg 122.

Core, section, interval (cm)	Depth (mbsf)	Volume (mL)	pH	Alkalinity (mM)	Salinity (‰)	Cl (mM)	Mg (mM)	Ca (mM)	Sr (mM)	Ba (μM)	Li (μM)	Na (μM)	K (mM)	Rb (mM)	SO_4 (mM)	SiO_2 (mM)	Fe (μM)	Mn (μM)
122-759B-																		
3R-3, 145–150	16.9	48	7.65	3.41	35.2	556	52.5	11.0	189	0.62	59.0	479	11.3	0.315	29.4	0.406	15.3	3.97
7R-1, 140–150	51.4	30	7.78	4.34	35.2	557	47.3	12.4	232	1.10	44.6	486	10.5	0.315	27.9	0.145	3.38	3.46
11R-1, 138–148	89.4	24	7.67	2.98	34.8	536	42.3	13.6	283	1.48	79.2	472	8.6	0.210	27.1	0.176	2.10	4.06
14R-1, 140–150	117.9	13	7.84	3.23	34.7	542	40.0	13.7	349	2.24	87.9	473	7.4	0.023	22.2	0.192	13.9	0.42
19R-2, 140–150	166.9	4			33.0	542	33.4	13.3	389	2.62	50.4	477	6.1	0.093	18.2	0.160		
24R-2, 140–150	214.4	45	7.42	2.37	34.7	559	29.8	13.7	501	0.91	47.5	508	4.6		19.9	0.109	0.75	4.46
27R-1, 140–150	236.9	10			33.6	558	26.7	13.6	514	1.55	36.0	503	4.2		15.9	0.137	1.86	5.84
34R-2, 140–150	272.9	8			33.0	558	27.1	14.2	599	4.28	59.0	501	4.2		15.8	0.198	1.95	6.06
122-760A-																		
1H-4, 140–145	5.9	45	7.72	3.11	35.4	556	51.5	11.2	174	0.36	31.7	480	10.9	0.725	28.4	0.531	13.2	3.55
2H-4, 140–145	13.6	35	7.70	2.90	35.5	559	49.1	11.9	206	0.34	46.1	482	11.8	0.643	26.4	0.554	15.6	1.87
3H-4, 140–145	23.1	50	7.65	2.98	35.6	566	48.3	13.2	230	0.31	44.6	491	10.3		27.8	0.221	1.92	3.84
4H-5, 140–145	34.1	40	7.50	2.77	35.7	564	45.9	14.4	277	0.29	41.7	490	9.8	0.702	26.3	0.207	2.04	9.47
5H-5, 140–145	43.6	50	7.68	2.85	34.5	559	43.6	14.7	285	0.32	33.1	488	9.8	0.643	26.0	0.319	1.29	15.1
6H-5, 140–145	53.1	30	7.64	2.89	34.5	561	41.4	15.1	294	0.40	38.9	495	9.5	0.585	26.3	0.229	0.59	15.3
7H-5, 140–145	62.6	20	7.59	2.86	34.3	564	42.2	15.8	308	0.34	50.4	494	8.7	1.076	25.7	0.161	0.86	12.8
8H-4, 140–145	70.6	25	7.52	2.75	35.5	568	41.7	16.0	338	0.36	43.2	500	9.4	0.397	26.9	0.173	0.50	32.2
9H-5, 140–145	81.6	20	7.60	2.90	34.5	558	39.2	15.9	340	0.70	48.9	492	8.2	0.444	24.6	0.254	0.98	39.0
10X-2, 140–145	86.6	3			32.6	521	43.4	16.5				447			23.1	0.286		
16X-4, 140–150	141.1	34	8.65	2.65	35.3	565	35.1	16.4	376	0.94	51.8	500	7.8	0.643	21.2	0.076	9.15	5.35
19X-2, 140–150	166.6	5			34.0	547	37.7	18.7				476			21.0	0.229	3.44	9.77
25X-4, 140–150	208.8	5			34.3	554	33.9	17.1	466	2.07	54.7	488	4.8	0.175	20.2	0.140		
30X-5, 140–150	239.8	4			33.0	559	30.7	17.2	506	1.79	38.9	495	4.6	0.198	17.7	0.132		
35X-3, 140–150	268.8	5			33.4	550	32.9	17.0	539	2.47	47.5	479	3.9	0.269	16.3	0.215		
122-760B-																		
10R-1, 140–150	322.4	10	7.95	2.58	33.2	561	14.9	13.4	941	1.85	86.4	527	2.5	0.128	11.0	0.166		
13R-2, 140–150	352.4	30	7.92	2.15	33.6	570	15.5	13.5	970	1.74	82.1	536	2.6	0.222	12.3	0.137	0.98	5.95
16R-3, 140–150	382.4	14	8.04	2.44	33.5	572	13.1	12.6	930	2.33	87.9	540	2.2	0.175	9.5	0.121	0.86	2.33
19R-2, 140–150	409.4	10	8.22	2.06	33.4	571	11.2	10.9			73.4	539	2.0	0.000	5.9	0.078		
22R-3, 140–150	439.4	10	8.22	1.88	32.7	576	10.0	9.8	908	2.94	33.1	547	2.0	0.315	5.2	0.063		
25R-2, 140–150	466.4	3			32.8	573	12.4	10.0	869	6.48	46.1	542	2.4	0.327	7.7	0.074		
Site 761 (surface)	0.0		8.44	2.60	35.0	550	53.9	10.3	132	0.03	27.3	472	10.0	1.474	28.9	0.004		
122-761B-																		
1H-2, 145–150	2.9	55	7.79	3.63	35.8	553	52.4	11.0	141	0.43	25.9	477	10.5	0.620	28.8	0.569	8.97	11.1
2H-5, 145–150	11.6	50	7.62	3.66	35.6	555	52.3	10.9	154	0.54	23.0	478	11.6	0.725	29.0	0.675	14.8	4.84
3H-5, 145–150	21.1	50	7.62	3.87	35.6	558	51.9	11.2	149	0.43	17.2	483	11.1	0.643	29.1	0.509	21.0	2.28
4H-5, 145–150	30.6	45	7.63	3.57	36.3	559	52.0	11.1	156	0.50	30.2	482	11.0	0.900	28.2	0.217	1.29	4.04
5H-5, 145–150	40.1	40	7.59	3.39	35.4	563	52.2	11.2	178	0.47	25.9	485	11.3	0.339	28.3	0.241	0.93	12.7
6H-5, 145–150	49.8	42	7.60	3.68	36.1	562	51.6	11.3	167	0.36	28.8	485	11.0	0.772	28.6	0.215	1.92	14.9
7H-5, 145–150	59.1	30	7.66	3.58	35.5	558	51.7	11.3	175	0.37	25.9	480	9.9	0.643	27.2	0.283	1.52	14.0
8H-5, 145–150	68.6	25	7.50	3.84	35.5	557	51.7	11.3	181	0.36	20.1	477	12.2	0.491	27.4	0.376	1.75	10.9
9H-5, 145–150	78.1	30	7.50	3.31	35.5	558	51.8	11.5	176	0.38	24.4	477	11.9	1.146	27.1	0.540	1.75	6.73
10H-5, 145–150	87.6	40	7.70	3.58	35.7	557	52.1	11.9	188	0.45	27.3	478	11.2	0.877	28.0	0.565	0.61	3.46
17X-4, 140–150	138.1	50	7.72	3.70	35.5	554	50.4	12.4	216	0.54	30.2	476	11.1	0.468	27.3	0.781	0.63	1.09
20X-3, 140–150	165.1	50	7.69	3.57	35.6	553	49.3	12.5	200	0.50	34.5	474	12.1	1.216	26.3	0.654	1.34	0.93
23X-4, 140–150	195.1	45	7.64	3.42	35.8	556	49.2	12.5	194	0.58	27.3	479	11.0	0.643	27.2	0.652	1.47	0.82
27X-2, 140–150	230.1	53	7.68	3.34	35.5	561	50.2	12.6	239	0.43	31.7	483	11.1	0.994	27.9	0.544	0.79	0.62
30X-2, 140–150	257.1	30	7.84	3.11	35.5	554	48.7	11.2	162	0.32		482	10.9		27.6	0.360	2.33	0.91
122-761C-																		
26X-2, 140–150	368.6	5			34.6	535	18.2	13.3	170	0.99	37.4		10.9	1.170	26.3	0.439		
31X-3, 140–150	412.6	4	7.00		33.8	510	15.0	15.6	240	1.71	48.9		6.0	0.222	26.1	0.186		
Site 762 (surface)	0.0		8.27	2.50	35.6	557	53.6	10.4	91	0.02	27.3	480	10.1	1.432	29.2	0.020		0.44
122-762A-																		
1H-2, 145–150	2.9	25	7.65	3.32	35.5		52.2	10.7	116	0.32	23.0		10.9	1.060	28.1	0.451	0.90	2.58
122-762B-																		
1H-2, 145–150	2.9	50	7.65	3.15	35.4	555	52.4	10.7	122	0.31	27.3	475	10.4	0.792	26.6	0.447	1.38	2.31
3H-4, 145–150	19.8	50	7.59	3.56	35.5	561	50.7	10.1	191	0.43	31.7	481	10.7	0.815	24.6	0.474	0.41	1.16
6H-5, 145–150	49.8	45	7.55	3.35	34.7	558	47.0	9.7	286	0.43	41.7	479	10.2	0.722	20.8	0.191	2.01	0.95
9H-5, 145–150	78.3	40	7.55	3.08	34.0	556	44.6	10.2	366	0.43	54.7	476	9.7	0.710	18.1	0.182	7.07	0.86
12H-1, 0–10	99.4	70	7.64	3.81	34.4	559	43.0	11.1	386	0.50	59.0	481	9.2	0.384	17.5	0.270	41.2	0.91
12H-5, 145–150	106.8	30	7.50	3.38	34.2	556	42.8	10.7	362	0.45	59.0	479	9.0	0.652	17.6	0.189	5.98	0.64
15H-5, 145–150	135.3	35	7.53	3.98	34.0	558	41.5	11.8	372	0.54	64.8	479	9.0	0.372	16.5	0.201	0.97	5.79
18H-1, 0–10	156.4	70	7.55	4.53	34.0	560	40.1	12.4	416	0.53	80.7	483	9.2	0.465	16.4	0.434	16.5	7.21
18H-5, 145–150	163.8	30	7.47	4.32	34.3	557	39.9	12.4	369	0.72	67.7	480	9.1	0.407	16.3	0.386	1.15	7.77
122-762C-																		
4X-3, 145–150	193.4	25	7.26	4.33	34.3	554	38.4	12.8	363	0.61	66.2	476	9.1	0.489	14.4	0.829	13.5	1.31
7X-3, 145–150	221.9	35	7.30	4.47	34.0	559	37.5	12.7	378	0.60	86.4	481	8.3	0.489	13.4	0.655	22.4	0.73
10X-4, 145–150	251.9	35	7.32	4.12	33.8	554	36.8	12.4	392	0.74	102.3	477	8.4	0.384	13.1	0.649	23.3	0.93
14X-5, 145–150	291.4	28	7.29	4.14	33.5	555	35.2	12.3	411	0.65	110.9	479	8.3	0.594	11.8	0.594	10.8	0.78
17X-4, 145–150	318.4	24	7.30	3.95	32.7	558	34.3	12.2	412	0.91	103.7	483	7.3	0.396	10.9	0.630	19.5	0.93

Table 1 (continued).

Core, section, interval (cm)	Depth (mbsf)	Volume (mL)	pH	Alkalinity (mM)	Salinity (‰)	Cl (mM)	Mg (mM)	Ca (mM)	Sr (mM)	Ba (μM)	Li (μM)	Na (μM)	K (mM)	Rb (mM)	SO$_4$ (mM)	SiO$_2$ (mM)	Fe (μM)	Mn (μM)
20X-2, 145–150	343.9	28	7.39	5.16	33.0	559	32.9	12.1	459	0.76	144.1	486	6.8	0.419	9.6	0.759	8.52	0.69
23X-2, 140–150	372.4	17	7.25	4.09	33.2	556	32.8	13.0	422	1.09	106.6	475	6.5	0.302	7.0	0.723	0.32	0.71
26X-4, 140–150	403.9	34	6.90	9.63	33.2	555	25.2	18.2	425	2.38	126.8	492	5.6	0.244	10.2	1.126	0.84	0.58
29X-2, 140–150	424.4	19	7.22	4.73	32.9	557	27.5	15.4	452	2.35	122.4	485	5.7	0.198	7.7	0.838	3.03	0.75
32X-2, 140–150	452.9	15	7.36	5.37	32.5	551	27.1	14.5	560	1.97	113.8	482	5.4		7.4	0.696	0.47	0.69
35X-1, 140–150	479.9	13	7.17	4.90	32.5	551	25.2	16.1	498	3.37	134.0	484	5.0	0.256	7.8	0.857	1.63	1.07
44X-4, 140–150	569.9	34	7.26	4.47	31.7	545	19.9	15.2	531	42.23	144.1	481	3.6	0.069	3.1	0.768	0.52	0.67
47X-5, 140–150	599.9	28	7.32	4.08	31.6	542	20.6	13.8	506	9.83	132.5	479	3.5	0.198	3.2	0.340	2.44	0.78
50X-2, 140–150	623.9	9	7.24	2.24	31.0	545	18.4	14.4	447	124.51	123.9	481	2.7	0.116	1.6	0.225		
53X-4, 140–150	655.4	11	7.17	3.22	31.0	538	17.9	14.3	517	18.78	148.4	478	3.2	0.250	2.6	0.238		
56X-5, 140–150	685.4	29	7.50	2.00	30.7	537	16.4	12.7	452	14.05	136.9	483	3.5	0.163	3.4	0.188	0.86	0.96
59X-4, 140–150	712.4	34	7.44	2.57	30.5	529	15.4	12.6	501	22.57	138.3	481	3.5	0.221	5.0	0.250	5.41	0.49
62X-4, 140–150	740.9	20	7.42	2.74	30.7	535	15.0	13.7	410	8.81	126.8	482	3.5	0.244	2.9	0.344	1.67	0.49
66X-4, 140–150	770.9	30	7.37	2.87	30.4	535	12.9	14.0	426	60.21	131.1	484	3.0	0.244	1.8	0.427	0.82	0.40
72X-1, 140–150	796.4	0.5			30.5	526									2.3	0.179		
82X-3, 140–150	857.9	3	7.35		28.2	491	11.3	12.5							1.9	0.150		
86X-3, 140–150	886.9	9	7.45	6.61	28.4	502	9.4	13.1	480	391.75	201.7	467	2.0	0.128	2.6	0.213		
89X-4, 140–150	916.9	5			28.4	495	11.6	12.8	476	24.53	178.7	441	1.8	0.256	2.1	0.273		
Site 763 (surface)		0.0	8.16	2.28	35.5	559	54.2	10.5	92	0.07	26.6	480	10.1	1.567	29.6	0.002	0.07	0.47
122-763A-																		
1H-2, 145–150	2.9	50	7.59	3.36	35.8	555	52.8	10.7	135	0.36	41.7	476	11.3	0.351	28.0	0.489	8.52	2.66
2H-4, 145–150	10.8	54	7.46	3.76	35.6	556	50.6	10.4	207	0.91	31.7	477	12.1	0.830	25.9	0.579	1.43	1.46
3H-4, 145–150	20.3	49	7.36	3.89	35.2	556	48.4	9.8	221	0.38	28.8	479	10.8	0.409	23.6	0.571	1.33	0.98
4H-4, 145–150	29.8	47	7.45	4.04	35.1	559	47.0	9.4	268	0.38	23.0	486	10.7	0.526	23.8	0.450	0.81	0.98
5H-4, 145–150	39.3	50	7.46	3.85	34.6	556	45.2	9.0	326	0.62	27.3	480	10.7	0.526	19.9	0.331	4.66	0.80
6H-4, 145–150	48.8	40	7.44	3.02	34.5	556	43.4	8.8	356	0.45	36.0	481	10.2	0.725	18.9	0.253	9.65	1.11
7H-1, 0–10	52.4	55	7.66	3.65	34.5	559	43.4	9.0	357	0.06	23.0	487	8.7	0.345	19.0	0.227	10.2	0.98
7H-4, 145–150	58.3	40	7.44	3.44	34.6	559	42.1	8.9	398	0.72	43.2	485	9.7	0.514	17.3	0.202	9.87	0.86
8H-4, 145–150	67.8	40	7.41	3.33	34.3	559	41.2	8.7	442	1.04	47.5	485	9.5	0.468	16.6	0.180	1.20	1.00
9H-4, 145–150	77.3	38	7.41	3.14	33.9	556	40.5	8.7	467	0.93	41.7	483	9.6	0.456	16.4	0.167	9.20	0.66
10H-4, 145–150	86.8	37	7.46	2.99	33.8	556	39.3	8.7	476	1.12	43.2	482	9.8	0.315	15.3	0.159	5.55	0.58
11H-1, 0–10	90.4	65	7.63	3.12	33.9	559	39.8	8.9	500	0.45	40.3	484	9.1	0.409	14.7	0.196	9.94	0.78
13H-4, 145–150	115.3	36	7.50	3.53	33.8	556	37.9	9.0	484	1.10	41.7	482	8.8	0.362	13.1	0.145	4.62	0.86
16H-4, 145–150	143.8	33	7.48	3.17	33.7	560	38.6	8.4	481	0.78	41.7	486	9.1	0.432	13.7	0.151	3.49	2.52
17H-1, 0–10	147.4	60	7.63	2.73	34.2	562	43.1	8.8	419	0.33	40.3	492	8.9	0.327	20.9	0.098	0.75	1.29
19H-4, 145–150	172.3	25	7.57	3.75	33.8	561	37.2	7.3	467	1.21	40.3	489	9.8	0.491	12.4	0.231	2.63	1.75
122-763B-																		
3X-4, 145–150	205.4	35	7.62	6.16	33.5	562	36.1	8.3	493	0.89	40.3	495	8.9	0.432	12.8	0.598	1.97	0.78
6X-4, 145–150	233.9	21	7.49	6.65	32.8	557	34.5	8.5	467	2.01	48.9	487	7.9	0.374	9.0	0.420	2.74	0.71
9X-4, 145–150	262.4	24	7.44	7.37	32.7	557	31.3	8.6	493	3.31	53.3	483	7.5	0.292	3.9	0.356	5.64	1.09
12X-3, 140–150	289.4	36	7.30	7.94	32.3	556	28.5	8.9	486	85.01	51.8	487	7.8	0.526	3.6	0.414	6.34	0.56
15X-4, 140–150	319.4	41	7.36	8.54	32.3	559	26.8	9.9	467	564.33	57.6	488	7.4	0.549	1.4	0.383	1.83	0.47
18X-3, 140–150	346.4	21	7.36	7.42	32.3	557	25.6	10.3	411	467.85	64.8	496	7.0	0.514	6.1	0.335	2.69	1.42
24X-5, 140–150	406.4	43	7.56	5.94	32.2	558	24.4	10.7	335	302.55	83.5	488	6.3	0.245	0.7	0.764	4.46	3.29
27X-4, 140–150	433.4	20	7.34	4.91	32.1	557	25.2	10.4	279	10.98	87.1	498	6.0	0.503	7.1	0.700	9.96	5.24
30X-4, 140–150	461.9	22	7.32	4.46	32.1	556	24.2	10.7	299	41.50	102.3	488	5.7	0.280	1.9	0.774	9.63	5.59
33X-5, 140–150	491.9	15	7.32	4.00	32.0	556	23.9	10.8	271	22.79	92.2	490	5.3	0.280	2.8	0.787	1.45	6.90
36X-4, 140–150	518.9	22	7.57	2.02	31.8	551	22.7	10.3	278	32.03	102.3	491	4.7	0.456	4.8	0.505	1.86	5.35
42X-6, 140–150	578.9	5			31.5	539	23.9	13.3	308	23.70	136.9		3.5	0.163	3.4	0.374		
45X-3, 140–150	602.9	7	7.01	2.96	31.7	539	24.3	13.8	297	9.10	145.5	481	3.2	0.210	9.3	0.279		
50X-4, 140–150	638.4	7	7.66	3.79	30.9	537	20.0	13.9	340	97.57	178.7	475	3.6	0.105	3.3	0.262		
122-763C-																		
6R-1, 140–150	662.0	7	7.55	3.99	31.7	535	22.4	14.3	306	13.81	180.1	469	2.7	0.081	3.6	0.181		
10R-4, 140–150	691.0	10			31.6	539	22.4	14.0	292	9.73	184.4		3.3	0.257	6.2	0.187	3.87	1.51
13R-4, 140–150	719.5	5			31.9	539	20.3	14.6	304	11.17	181.5		2.8	0.304	3.5	0.175		
16R-5, 140–150	749.5	9	7.10	3.08	31.8	540	18.2	14.7	315	30.37	171.4	481	2.4	0.210	3.6	0.152	14.5	2.28
19R-4, 140–150	776.5	10	7.50	3.06	30.5	536	17.4	14.8	337	228.85	158.5	477	2.2	0.163	2.8	0.135	2.11	1.44
22R-4, 140–150	814.5	12	7.58	3.13	31.5	539	21.0	14.8	293	21.69	134.0	485	2.6	0.187	8.9	0.137	0.63	1.07
25R-5, 140–150	844.5	2			31.5	539	20.1	15.6	317	22.08	152.7		2.4	0.117	6.2	0.162		
28R-4, 140–150	871.5	7	7.34	2.95	31.7	533	19.8	15.8	333	8.45	136.9	472	2.2	0.245	5.3	0.187		
32R-5, 140–150	901.5	9	7.45	3.27	31.2	532	19.8	15.1	307	15.60	123.9	469	2.1	0.187	3.2	0.175		
34R-5, 140–150	930.0	2	7.46		31.8	534	21.3	15.9	302	16.74	158.5		3.0		9.2	0.216		
41R-4, 140–150	995.0	1			30.5	535			315	24.46			2.6	0.269	7.4	0.137		

possibly four Fe and Mn maxima were observed at Sites 762 and 763. The Mn maxima overlie those of Fe as expected on the basis of their respective redox chemistries. However, the maxima at Site 762 are much less pronounced than at Site 763.

A small dissolved Mn maximum of approximately 2.5 μmol/L immediately below the sediment surface is followed by a decrease to less than 1 μmol/L between 50 and 100 mbsf. Well-delineated Mn maxima occur near 150–175 mbsf, below which concentrations are again less than 1 μmol/L. The dissolved Fe profile at Site 762 is offset slightly deeper within the sediments at Site 762 (near 75 mbsf) relative to Site 763, but profiles appear to correlate well farther downhole.

Table 2. Major element composition of Leg 122 sediments.

Core, section, interval (cm)	Mg (mg/g)	Ca (mg/g)	Sr (mg/g)	Ba (mg/g)	Si (mg/g)	Al (mg/g)	Ti (μg/g)	Fe (mg/g)	Mn (mg/g)	Li (μg/g)	K (mg/g)	Depth (mbsf)
Site 759												
122-759B-												
3R-3, 145–150	3.67	328.8	1.26	0.597	35.5	15	571	9.4	0.21	122		16.9
7R-1, 140–150	6.72	16.5	0.24	0.385	310.0	79	5620	32.1	0.23	39	30.1	51.4
11R-1, 138–148	8.27	2.6	0.11	0.434	463.7	90	4274	31.1	0.08	44	27.1	89.4
14R-1, 140–150	8.96	3.7	0.18	0.447	302.0	106	5580	38.0	0.97	22	21.1	117.9
19R-2, 140–150	8.67	2.4	0.13	0.432	295.5	96	4965	27.8	0.28	48	30.4	166.9
24R-2, 140–150	8.04	5.2	0.18	0.462	327.5	78	3505	28.1	0.44	30	23.8	214.4
27R-1, 140–150	8.54	3.9	0.15	0.423	285.0	85	4640	34.1	0.63	43	25.7	236.9
34R-2, 140–150	9.89	13.7	0.19	0.312	249.0	100	4690	72.2	1.13	60	23.6	272.9
Site 760												
122-760A-												
1H-4, 145–150	2.03	370.9	1.50	0.570	22.6	8	354	4.5	0.15	8		5.9
2H-4, 145–150	5.00	307.3	1.36	0.933	45.0	20	767	11.9	0.17	18		13.6
3H-4, 145–150	2.83	360.7	1.10	0.497	17.0	7	258	3.3	0.41	6		23.1
4H-5, 145–150	5.19	355.5	1.04	0.114	24.8	8	293	4.2	0.42	6		34.1
5H-5, 145–150	7.26	309.4	0.96	0.205	48.7	20	675	10.5	0.65	17		43.6
6H-5, 145–150	1.42	367.3	1.19	0.234	13.9	6	234	3.9	0.54	5		53.1
7H-5, 145–150	3.44	282.5	1.04	0.254	64.3	29	1088	14.4	0.22	23		62.6
8H-4, 145–150	1.74	374.5	1.11	0.822	11.6	2	129	4.4	0.44	4		70.6
9H-5, 145–150	8.37	5.2	0.17	0.817	286.0	71	3870	72.3	5.34	13	25.2	81.6
10H-2, 145–150	6.43	1.9	0.10	0.312	304.0	124	5350	31.9	0.11	58	20.9	86.6
16X-4, 140–150	2.19	1.6	0.11	0.548	364.5	62	4575	15.2	0.15	16	25.6	141.1
19X-2, 140–150	5.05	1.5	0.12	0.416	322.0	97	6840	23.6	0.11	53	30.5	166.6
25X-4, 140–150	4.30	1.2	0.24	0.507	261.0	101	5410	18.1	0.20	47	32.2	208.8
30X-5, 140–150	8.86	2.6	0.14	0.407	276.0	101	5100	41.1	0.32	53	24.6	239.8
35X-3, 140–150	7.58	47.3	0.68	0.239	227.0	86	5260	38.6	0.36	66	25.0	268.8
37X-CC, 0–5	8.97	39.3	0.45	0.286	227.0	100	5130	40.6	0.29	70	27.3	283.9
122-760B-												
10R-1, 140–150	8.53	3.5	0.33	0.433	288.0	90	5110	38.7	0.74	76	21.1	322.4
13R-2, 140–150	6.79	3.8	0.20	0.456	303.0	86	4350	28.6	0.41	53	23.5	352.4
16R-3, 140–150	8.80	3.2	0.22	0.447	282.0	96	5320	33.9	0.43	72	31.5	382.4
19R-2, 140–150	8.04	5.0	0.17	0.462	333.0	78	3440	28.1	0.44	30	23.8	409.4
22R-3, 140–150	7.65	4.2	0.25	0.451	308.0	87	4790	31.1	0.30	44	24.4	439.4
25R-2, 140–150	7.24	4.1	0.23	0.485	302.5	96	5580	30.6	0.54	53	22.3	466.4
28R-2, 140–150	7.59	5.0	0.24	0.506	293.0	91	4780	35.6	1.24	48	24.9	489.9
Site 761												
122-761B-												
1H-2, 145–150	2.59	330.7	1.41	0.666	44.1	12	671	6.3	0.33	11		3.0
2H-5, 145–150	3.90	320.7	1.38	0.985	45.4	17	759	8.5	0.26	16		11.7
3H-5, 145–150	4.16	310.3	1.35	0.880	47.0	20	853	10.5	0.24	16		21.2
4H-5, 145–150	2.87	355.8	1.35	0.400	23.2	10	413	5.4	0.31	9		30.7
5H-3, 145–150	6.43	327.8	1.09	0.111	39.3	15	430	7.8	0.39	13		40.2
6H-5, 145–150	4.11	328.1	1.03	0.173	32.1	16	721	9.5	0.70	16		49.2
7H-5, 145–150	2.29	358.9	1.23	0.192	29.2	11	440	7.0	0.52	8		59.2
8H-5, 145–150	1.59	365.6	0.97	0.704	9.4	2	87	2.3	0.15	2		68.7
9H-5, 145–150	1.90	371.1	1.05	0.607	13.6	3	103	4.1	0.15	4		78.2
10H-5, 145–150	2.45	366.4	1.05	0.903	29.7	5	222	8.4	0.18	4		87.7
17X-4, 140–150	2.24	349.9	1.14	0.717	30.5	6	149	3.1	0.12	10		138.1
20X-3, 140–150	2.41	335.5	0.80	0.541	42.0	9	263	4.6	0.16	10		165.1
23X-4, 140–150	3.09	343.2	1.00	0.835	29.7	8	213	4.9	0.11	14		195.1
27X-2, 140–150	2.11	370.6	0.57	4.007	17.3	4	235	3.3	0.20	2		230.1
30X-2, 140–150	8.50	20.8	0.18	0.456	291.0	53	9330	75.0	0.66	11	29.7	257.1
122-761C-												
26R-2, 140–150	11.40	141.0	0.45	0.156	194.0	55	3330	26.9	0.46	24	26.5	368.6
31R-3, 140–150	11.10	187.0	1.27	0.124	139.0	60	3300	29.6	0.57	26	17.6	412.6
Site 762												
122-762A-												
1H-2, 145–150	2.89	342.3	1.45	0.364	24.0	9	387	5.4	0.19	12		3.0
122-762B-												
1H-2, 145–150	2.81	343.5	1.40	0.344	23.4	8	301	6.1	0.18	8		3.0
3H-4, 145–150	3.43	339.2	1.52	0.360	23.7	9	347	6.1	0.20	12		19.9
6H-5, 140–150	2.87	332.3	1.47	0.388	30.9	14	510	12.5	0.30	13		49.9
9H-5, 145–150	2.64	347.5	1.48	0.334	26.8	13	525	6.7	0.31	11		78.4
12H-5, 145–150	1.88	353.3	1.50	0.213	17.8	9	308	4.5	0.15	8		106.9
15H-5, 140–150	3.11	351.8	0.78	0.041	20.7	9	375	7.3	0.23	11		135.4
18H-5, 145–150	2.04	332.2	1.04	0.260	28.2	8	337	8.8	0.19	5		163.9
122-762C-												
4X-3, 145–150	1.40	374.1	1.38	0.308	19.8	3	131	2.0	0.15	3		193.5
7X-3, 145–150	1.45	356.8	1.65	0.441	24.7	5	212	3.2	0.19	6		222.0
10X-3, 145–150	1.57	352.2	1.35	0.463	19.9	4	188	3.3	0.14	5		250.5

Table 2 (continued).

Core, section, interval (cm)	Mg (mg/g)	Ca (mg/g)	Sr (mg/g)	Ba (mg/g)	Si (mg/g)	Al (mg/g)	Ti (μg/g)	Fe (mg/g)	Mn (mg/g)	Li (μg/g)	K (mg/g)	Depth (mbsf)
14X-5, 145–150	2.46	331.9	1.13	0.700	36.6	7	332	10.8	0.18	5		291.5
17X-4, 145–150	2.18	355.5	0.92	0.730	23.6	4	219	8.1	0.18	2		318.5
20X-2, 145–150	2.03	361.8	0.71	1.207	22.9	5	159	5.9	0.22	2		344.0
23X-2, 145–150	2.45	345.1	0.78	0.969	31.3	8	271	7.2	0.33	7		372.4
26X-4, 140–150	1.85	327.6	0.92	0.873	48.0	7	313	4.0	0.19	3		403.9
29X-2, 140–150	2.65	349.0	1.13	0.404	37.3	11	291	10.9	0.12	9		424.4
32X-2, 140–150	1.43	349.1	1.28	0.544	24.3	6	231	3.0	0.09	7		452.9
35X-1, 140–150	3.24	304.3	0.99	0.569	47.0	14	467	7.3	0.13	14		479.9
44X-4, 140–150	1.53	360.2	0.92	0.795	15.1	4		3.1	0.18	7		569.9
47X-5, 140–150	1.42	358.5	1.11	0.827	14.6	5	245	3.4	0.24	6		599.9
50X-2, 140–150	2.32	342.0	0.95	0.977	36.3	12	577	8.2	0.31	9		623.9
53X-4, 140–150	2.88	311.6	0.86	1.701	49.7	21	975	15.2	0.28	26		655.4
56X-5, 140–150	2.92	322.6	0.85	3.203	46.9	17	653	10.8	0.18	22		685.4
59X-4, 140–150	1.54	368.1	0.82	3.026	15.5	4	211	3.7	0.11	3		712.4
62X-4, 140–150	1.39	388.5	0.67	0.077	10.2	2	131	2.1	0.10	2		740.9
66X-4, 140–145	1.28	381.4	0.73	2.254	10.8	2	106	2.2	0.13	5		770.9
72X-1, 140–150	3.02	331.5	0.62	9.008	36.1	11	740	10.4	0.28	8		796.4
77X-6, 140–150	3.70	322.3	0.29	0.837	47.3	12	801	7.0	0.70	10		829.0
82X-3, 140–150	9.57	3.7	0.20	0.857	226.0	96	6330	78.6	0.34	134	34.2	857.9
86X-3, 140–150	8.23	3.4	0.14	0.818	247.6	109	5888	61.3	0.31	134	36.7	886.9
89X-4, 140–150	8.86	3.7	0.15	0.717	259.8	101	5607	66.8	0.24	130	31.9	916.9
89X-4, 140–150	8.43	3.5	0.14	0.581	251.3	94	5554	65.2	0.32	130	31.4	916.9
Site 763												
122-763A-												
1H-2, 145–150	2.74	359.4	1.51	0.426	23.1	8	371	5.4	0.23	7		3.0
2H-4, 145–150	2.31	347.1	1.47	0.399	27.8	7	271	4.4	0.15	8		10.9
3H-4, 145–150	2.71	357.7	1.52	0.371	24.2	7	300	4.6	0.17	8		20.4
4H-4, 145–150	4.65	321.4	1.37	0.379	34.6	14	511	8.7	0.20	15		29.9
5H-4, 145–150	2.81	354.9	1.60	0.338	21.6	9	396	5.0	0.20	10		39.4
6H-4, 145–150	2.97	341.9	1.63	0.396	25.5	11	403	6.4	0.24	10		48.9
7H-4, 145–150	3.05	327.2	1.52	0.415	32.0	14	492	8.4	0.33	10		58.4
8H-4, 145–150	3.12	337.6	1.53	0.460	33.2	16	533	10.1	0.34	11		67.9
9H-4, 140–150	2.56	331.0	1.57	0.249	25.1	12	447	7.3	0.26	13		77.4
10H-4, 140–150	2.30	355.4	1.01	0.967	19.0	5	207	4.4	0.09	4		86.9
13H-4, 140–150	1.87	360.9	1.44	0.211	14.7	6	226	7.1	0.15	5		115.4
16H-4, 145–150	2.87	358.9	1.06	0.098	13.9	5	208	2.9	0.29	4		143.9
19H-4, 145–150	2.00	324.2	1.06	0.321	33.5	10	477	8.6	0.29	6		172.4
122-763B-												
3X-4, 145–150	1.51	352.0	1.53	0.525	24.5	6	260	3.1	0.12	2		205.5
6X-4, 145–150	2.17	354.7	1.38	0.255	18.2	8	308	5.0	0.22	9		234.0
9X-4, 145–150	3.91	316.7	0.86	2.555	49.5	17	715	12.9	0.33	16		262.5
12X-3, 140–150	2.38	349.4	0.94	2.964	26.5	8	347	5.6	0.06	7		289.4
15X-4, 140–150	3.52	376.6	0.72	2.238	14.0	3	182	3.5	0.02	3		319.4
18X-3, 140–150	3.67	318.0	0.58	3.920	38.4	15	604	9.3	0.25	16		346.4
24X-5, 140–150	4.53	199.4	0.83	2.320	132.3	28	1314	16.2	1.06	15		406.4
27X-4, 140–150	4.77	115.7	0.43	0.851	239.2	25	1409	47.1	1.51	12		433.4
30X-4, 140–150	9.33	137.8	0.49	2.196	198.0	39	1740	21.0	2.49	22		461.9
33X-5, 140–150	6.70	149.7	0.52	1.703	179.0	32	1624	15.1	0.89	17		491.9
36X-4, 140–150	5.82	208.4	0.36	1.383	120.4	29	1252	20.4	1.79	15		518.9
37X-1, 47–50	8.89	180.2	0.40	1.301	174.9	40	2438	26.3	0.92	26		523.0
37X-2, 42–45	7.72	198.2	0.39	1.653	162.2	36	2165	21.1	0.79	22	13.5	524.4
37X-3, 47–50	6.02	263.0	0.35	1.017	112.5	23	1562	16.1	1.11	19		525.9
37X-4, 47–50	5.47	239.9	0.37	1.335	131.3	25	1554	14.2	0.92	18	10.1	527.4
37X-5, 52–55	9.04	149.0	0.34	1.948	198.8	47	2528	24.0	0.60	38	16.4	528.9
38X-7, 46–49	5.78	271.2	0.36	0.459	108.0	21	1465	15.4	0.89	22	7.4	532.4
39X-1, 47–50	4.05	142.0	0.20	0.357	272.2	15	1101	11.2	0.43	14	5.0	542.0
40X-1, 50–53	3.10	79.9	0.15	0.404	328.5	13	1030	8.1	0.16	6	4.3	551.5
40X-2, 50–53	3.74	45.8	0.12	0.593	365.2	18	1525	13.2	0.16	6	6.9	553.0
41X-2, 47–49	5.45	66.6	0.18	1.166	310.0	28	2146	21.2	0.39	20	10.7	561.0
42X-2, 45–49	10.36	3.5	0.23	2.819	325.6	58	3519	41.4	0.33	48	21.9	562.5
42X-3, 44–50	10.49	2.3	0.23	3.210	319.3	61	3407	39.7	0.29	53	20.8	564.0
42X-4, 45–49	12.68	2.4	0.22	2.639	319.4	66	3971	41.8	0.26	55	20.7	565.5
42X-5, 46–51	9.44	3.2	0.24	3.071	317.4	56	3440	39.1	0.26	39	22.1	567.0
42X-6, 47–51	8.56	3.9	0.24	2.897	332.9	54	3358	41.4	0.54	39	22.5	568.5
42X-6, 140–150	10.40	4.5	0.19	2.311	326.6	60	3657	43.8	0.36	42	22.5	578.9
42X-74, 7–52	9.97	3.1	0.20	2.466	318.1	56	3515	43.5	0.37	44	20.9	579.4
43X-1, 44–47	10.38	6.3	0.27	3.620	313.2	62	3482	32.7	0.28	49	18.9	580.0
43X-3, 48–50	10.90	18.5	0.26	3.334	303.2	66	3552	32.3	0.19	52	20.6	583.0
43X-4, 48–52	10.59	2.2	0.21	2.457	320.9	62	3546	38.1	0.15	50	21.3	584.5
45X-3, 140–150	13.54	10.2	0.24	2.746	305.3	70	3030	34.1	0.13	62	18.5	602.9
47X-1, 47–49	5.93	94.4	0.24	1.443	270.3	29	1982	24.9	0.59	27	11.9	618.0
50X-4, 140–150	7.21	3.6	0.10	0.756	269.3	86	7332	62.6	0.23	98	32.4	638.4
122-763C-												
6R-1, 140–150	6.84	2.5	0.12	0.662	290.4	90	6574	49.9	0.39	91	25.5	662.0
10R-4, 140–150	9.63	16.9	0.18	0.668	245.7	100	5770	58.4	0.38	121	29.3	691.0
13R-4, 140–150	8.46	3.1	0.11	0.705	267.9	102	5912	52.8	0.44	134	30.7	719.5

Table 2 (continued).

Core, section, interval (cm)	Mg (mg/g)	Ca (mg/g)	Sr (mg/g)	Ba (mg/g)	Si (mg/g)	Al (mg/g)	Ti (μg/g)	Fe (mg/g)	Mn (mg/g)	Li (μg/g)	K (mg/g)	Depth (mbsf)
16R-5, 140–150	8.45	4.9	0.11	0.673	278.1	96	6145	55.1	0.17	112	29.6	749.5
19R-4, 140–150	8.92	5.3	0.14	0.683	272.0	104	6295	51.2	0.27	133	31.0	776.5
22R-4, 140–150	10.14	4.1	0.13	0.664	257.2	104	6085	62.7	0.35	131	29.0	805.1
25R-5, 140–150	10.16	3.9	0.14	0.632	254.2	108	5723	60.7	0.32	144	22.4	835.1
28R-4, 140–150	9.44	3.2	0.11	0.656	323.0	100	6046	55.3	0.16	125	27.5	862.1
32R-5, 140–150	9.01	4.6	0.10	0.618	267.6	94	5499	62.0	0.30	106	27.5	892.1
34R-5, 140–150	10.38	4.7	0.13	0.631	257.6	107	5641	62.0	0.31	127	26.9	920.6
37R-5, 140–150	11.24	5.2	0.14	0.593	242.9	115	5789	62.3	0.36	127	25.3	949.1
41R-4, 140–150	9.72	3.1	0.12	0.648	259.1	113	7926	51.8	0.25	120	26.2	985.6

DISCUSSION

Wombat Plateau Sites

Vertical trends in the pore-water concentrations of Ca, K, Mg, Rb, Sr, and sulfate downhole reflect both diagenesis and the changing bulk sediment chemistry with increasing depth at Sites 759 and 760. The lack of significant pore-water concentration gradients at Site 761, except for silica, may be attributed largely to the erasure of diffusion profiles by circulation of seawater through predominantly unconsolidated (to weakly lithified) carbonate sediments. Gradients that provide evidence of sedimentary reactions involving silica, however, reflect the extremely reactive nature of this species and its greater dependence on the lithology of the sediments than other pore-water constituents (Gieskes, 1981, 1985).

Because Sites 759 and 760 appear to be more closely related in their sedimentary and pore-water compositions, they are discussed together. Pore-water constituent profiles are rather monotonous at Site 761 and will be discussed principally in terms of silica diagenesis and the occurrence of ferromanganese-rich deposits.

Calcium and Mg concentration gradients are generally opposite one another and reflect carbonate diagenesis. However, coincident variations below Unit III at Site 760 indicate that carbonate diagenesis does not solely control the concentration of these elements. The increasingly siliciclastic lithology in Units IV through VI (Haq, von Rad, O'Connell, et al., 1990) suggests that ion-exchange reactions in clays also influence the dissolved concentrations of Ca and Mg. Although a significant portion of the Mg uptake is attributed to the precipitation of dolomitic limestones, observed in Site 759 and 760 sediments (Haq, von Rad, O'Connell, et al., 1990), uptake of Mg during the formation of smectite can also be invoked to explain its behavior below Unit III of Site 760 (Kastner and Gieskes, 1976; Gieskes et al., 1981). At Site 761 dissolved Mg varies by less than 10% throughout the carbonate oozes and chalks of lithological Units I and II and the ferruginous sandstone of Unit III. It is only in Unit V that a large depletion of Mg is observed. Because of the lack of pore-water samples in Unit IV it is not possible to say at which depth the depletion of Mg becomes significant. Based on the lithology (Haq, von Rad, O'Connell, et al., 1990), Mg depletion may begin in Unit IV where limestones and authigenic clays (Thurow and von Rad, this volume) occur, and continue through the calcareous claystone and crinoidal limestone of Units V and VI. It is likely that extensive diffusion through the unconsolidated oozes and chalks of the upper section of Site 761 has smoothed out concentration gradients (Lasaga and Holland, 1976; Gieskes et al., 1981).

Positive dissolved Sr gradients creating approximately three-fold (Site 759) to 10-fold (Site 760) enrichments downhole result primarily from the recrystallization of carbonates. The extent of carbonate recrystallization was evaluated by calculating the δSr/δCa ratio within carbonate sediments. Variations in the dissolved concentration of these elements in siliciclastic sediments might result from other reactions, hence no calculation was performed in non-carbonate sediments. Elevated δSr/δCa ratios ($35-50 \times 10^{-4}$) in the pore water relative to the Sr/Ca ratio in nannofossil oozes (approximately 20×10^{-4}) provide evidence of recrystallization (Baker et al., 1982). In Units V through VII, at Site 760, carbonate recrystallization probably continues to increase dissolved Sr concentrations, but the greater abundance of siliciclastic sediments and ion-exchange reactions in clays may also affect the Sr abundance. Weaker positive dissolved Sr gradients within the unconsolidated carbonate sediments of Site 761 suggest a lesser extent of carbonate recrystallization. Overall, the changes in the pore-water concentrations of Ca, Mg, and Sr may be attributed to carbonate diagenesis and ion exchange reactions with clay minerals.

Barium does not correlate with the other alkaline earths. Dissolved Ba concentrations are controlled primarily by the solubility of $BaSO_4$ and are manifested by greater than 10-fold increases downhole. A decrease in concentration toward the seawater value near 214 mbsf at Site 759 is attributed to contamination of the sample with sulfate-enriched drilling water.

Weak sulfate gradients in the upper 80–100 mbsf, which steepen substantially below this depth, suggest limited sulfate reduction associated with the degradation of organic matter within this portion of the sediments, or substantial diffusion. Based on the lithology (Haq, von Rad, O'Connell, et al., 1990) and the amount of pore water squeezed (Table 1) from the recovered sediments (i.e., indicator of the extent of lithification of sediments), the latter explanation appears more plausible. Significantly lower sediment porosity below Units I and II at Sites 759 and 760 (Haq, von Rad, O'Connell, et al., 1990) limits diffusion and helps to maintain steeper sulfate gradients than in the unconsolidated oozes.

Below the oozes, changes in sulfate concentration gradients appear to roughly follow lithological boundaries. A relatively sharp decrease is observed within the Fe- and Mn-rich sediments of Unit III at Site 760, whereas a similar decrease at Site 759 is only apparent well within lithological Unit III. A minimum (5.2 mM sulfate) in lithological Unit VI (Site 760) is not associated with an alkalinity maximum, suggesting that the bicarbonate produced is consumed by precipitation of calcite (Couture et al., 1977; Gieskes et al., 1987). Sulfate depletion downhole is rather continuous at both sites, indicating that similar processes govern sulfate concentrations throughout the sediments. There is only a weak negative sulfate gradient at Site 761 (Fig. 2 and Table 1). This contrasts sharply with observations at Sites 759 and 760 (80% depletion near the bottom of the holes) and suggests extensive circulation of seawater throughout Site 761. Alternatively, the

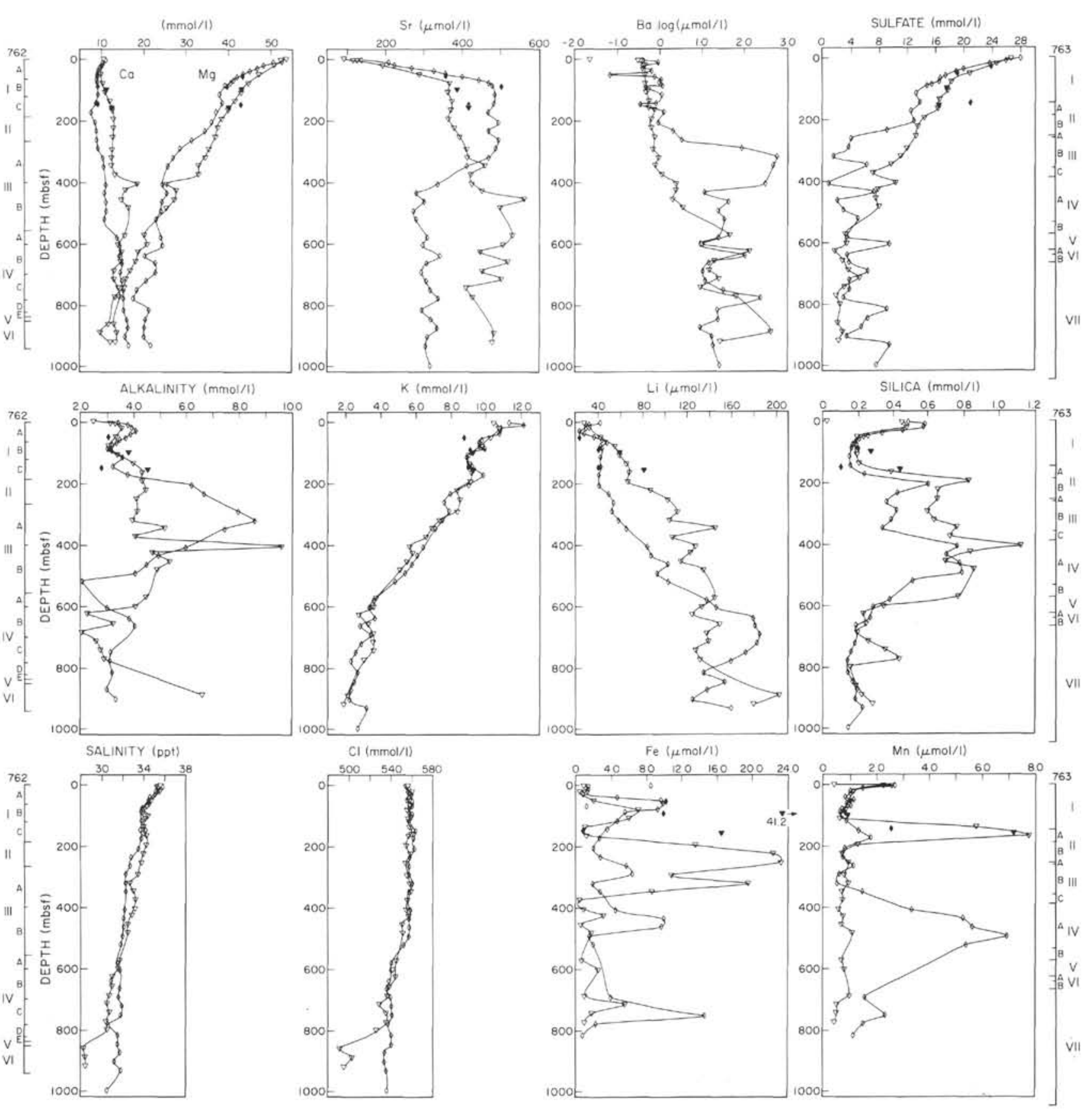

Figure 3. Exmouth Plateau sites: pore-water concentrations as a function of depth with lithological units indicated to the left. Triangles = Site 762, diamonds = Site 763. Closed symbols = "Barnes" harpoon samples; open symbols = squeezed pore-water samples

slight sulfate depletion could be explained by differences in the total organic carbon (TOC) content of the sediments (<0.10% above 348 mbsf at Site 761 vs. a range of approximately 1%–3% at Sites 759 and 760) (Haq, von Rad, O'Connell, et al., 1990).

The alkalinity profiles at all Wombat Plateau sites are characterized by slight decreases downhole. No significant increases expected as a result of the degradation of organic matter are apparent, although TOC contents of 1%–3% were observed at Sites 759 and 760. This suggests that any alkalinity produced during sulfate reduction is consumed by precipitation of carbonates. The low TOC content of Site 761 sediments above 348 mbsf is reflected in a nearly constant, although higher, alkalinity than at the previous two sites. This alkalinity increase is compatible with the slight extent of calcite dissolution and sulfate reduction evidenced by higher dissolved Ca and lower sulfate, respectively.

Except for the uppermost 20 to 30 mbsf, K and Mg profiles are similar. Increases in the K concentration within lithologic Unit I at all sites are likely due to temperature of squeezing effects (Bischoff et al., 1970). The onset of a negative K gradient below 400 mbsf at Site 761 coincides with a change in the lithology from predominantly marine carbonate-rich sediments (Subunit VA) to a greater proportion of clay-rich delta plain sediments (Subunits VB–VI) (e.g., Table 2; Haq, von Rad, O'Connell, et al., 1990; Wilkens et al., this volume).

The dissolved Li profiles at Sites 759 and 760 are influenced by diagenetic processes as well as by the presence of clays. There is a weak relationship between the dissolved Li and silica concentrations throughout most of the sediments. Within the carbonate oozes (Units I and II) Li concentrations may reflect its release during the dissolution of amorphous silica. Deeper downhole, however, the variations in dissolved Li correlate with changes in the lithology from carbonates to claystones, and likely result from uptake of Li by clay minerals. It should be noted that Li and silica profiles are completely decoupled at Site 761.

The large variations in dissolved silica throughout the Wombat Plateau sediments are likely due to silica diagenesis although no simple inverse relationship between silica and Ca or alkalinity, which would reflect silica diagenesis (Gieskes, 1981), exists in the sediments at Sites 759 or 760. Rather a relationship between Mg and SiO_2 at Site 760 is consistent with the uptake of Mg and SiO_2 during the formation of smectite (Kastner and Gieskes, 1976); however, the various fields in Figure 4 suggest that dissolved concentrations of these two species are influenced by different reactions in the various lithological units.

Much greater variability is noted in the dissolved silica concentrations at Site 761 (Table 1). A strong negative gradient within lithological Unit I coincides with the disappearance of radiolaria from the sediments (Schrader, 1972). From approximately 50 to 140 mbsf the strong positive gradient (0.643 mmol/L/100 m), with a maximum of 0.78 mmol/L at 138 mbsf, probably results from the dissolution of skeletal opal-A. It correlates with the transition from lithological Subunits IB to IC in which massive cherts exist (Haq, von Rad, O'Connell, et al., 1990) and reflects major SiO_2 mobilization and precipitation of authigenic silica. The gradual decrease to near 0.37 mmol/L at 257 mbsf and further to 0.186 mmol/L downhole is inferred to represent incorporation of silica into clay minerals (Kastner and Gieskes, 1976) or, perhaps, equilibrium with opal-CT. It coincides with the presence of dark laminated claystone in Subunit VB.

Decreases in pore-water salinity from the seawater value to approximately 32 g/kg can be largely attributed to the loss of K, Mg, and sulfate with increasing depth downhole. Salinity and dissolved Cl at Site 760 decrease most (35.5–32.6 g/kg and 568–521 mmol/L, respectively) between 82 and 86 mbsf near the boundary between lithological Unit III, a Mn oxide-rich sandstone and siltstone interval, and Unit IV sediments comprised of claystones with root-mottling and minor coal. The sympathetic Cl and salinity changes throughout Units III and IV suggest a freshwater intrusion near the top of Unit IV. However, Gieskes (1974) has indicated that an input of freshwater should only be considered if the salinity drops below 31.5 g/kg. At Site 760 there is no correlation between sediment porosity and Cl or salinity. The porosity at the boundary of Units II and III is near 70%, it is near 60% at 82 mbsf, and approximately 50% at 86 mbsf and decreases further throughout Unit IV (Haq, von Rad, O'Connell, et al., 1990). Greater freshwater flow would be expected through the upper section of Unit III than near the boundary of Units III and IV. Chloride increases below Unit IV, whereas a loss of K, Mg, and sulfate leads to a salinity decrease. Hence, the less saline waters at 86 mbsf are a localized occurrence within the sedimentary column that may result from horizontal advection of fresh waters from the Australian continent. Similar occurrences of lateral transport of fluids (both more and less saline than seawater) at depth have been reported previously and are generally associated with sands or siltstones (Couture et al., 1977; Gieskes, 1981).

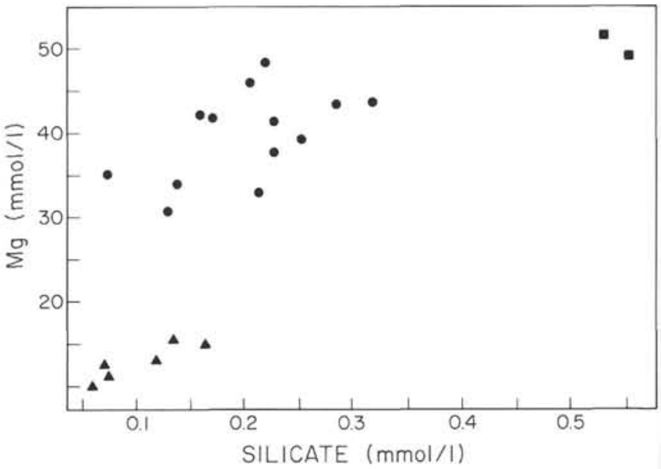

Figure 4. Mg vs. SiO_2 at Site 760. Squares = Unit I, circles = Units II–V, and triangles = Units VI and VII.

Dissolved Fe and Mn profiles appear to reflect changes in redox conditions within the first 50 mbsf of the sediments (Fig. 2 and Table 1). Elevated Mn concentrations immediately below the sediment/seawater interface and higher Fe concentrations from about 5–20 mbsf follow the conventional redox sequence associated with the degradation of organic matter in sediments. A large dissolved Mn maximum (39 μmol/L) at 81.6 mbsf (Site 760) coincides with the occurrence of ferromanganese-rich sediments and crusts in lithological Unit III (e.g., De Carlo and Exon, this volume). A smaller, yet well-defined, maximum is also observed at 50 mbsf in the sediments of Site 761, although no Fe-Mn-rich sediments were found that could explain the higher dissolved Mn concentrations. Pore waters from the Wombat Plateau sites generally exhibit an increase in dissolved Fe immediately below the Mn maxima, although the former is quite small at Site 761, and no downhole Mn maximum is observed at Site 759. The local maximum of approximately 9 μmol/L Fe associated with a pH of 8.65 at 141 mbsf in Unit IV of Site 760 is unusual, particularly considering the high pH, and the reason for this remains unclear. The low pore-water Fe and much higher Mn concentrations in Unit III suggest that redox conditions are suboxic within this interval, but are not sufficiently reducing to cause dissolution of Fe oxides. The dissolved Fe and Mn profiles of Site 761 suggest that variable redox conditions exist over the first 80 mbsf. Although no obvious Fe-Mn-rich intervals were noted in the core descriptions, white, brown, and gray layers occur over 10- to 30-cm intervals and extend to the lower boundary of Subunit IA in Core 122-761B-8H. Colored layers were also observed in Subunit IB to 90.5 mbsf (Haq, von Rad, O'Connell, et al., 1990), below which the concentrations of these metals return to background levels. The color banding may reflect variable redox conditions although shipboard descriptions suggest that the color changes are associated with variations in the ratio of foraminifers to nannofossils in the sediments.

Sites 762 and 763

The strong negative Mg gradient is not as pronounced in the upper 100 m of Site 762 as in the corresponding section of Site 763. However it is, on average, almost linear down to approximately 800 and 500 mbsf at the two sites, respectively. These depths correspond roughly to the limit below which the sediments are more lithified or grade from predominantly carbonates to a greater abundance of siliciclastic matter (Haq, von Rad, O'Connell, et al., 1990). Much smaller Mg gradients exist below these depths, suggesting that the Mg diffusion profile is strongly affected by the extent of carbonate sedimentation. The existence of at least three changes in slope in the dissolved Mg profile in the carbonate sequence of Site 763 reflects changes in the lithology, hence, porosity of the sediments, that are more pronounced than at Site 762. Concentration reversals noted in the lower 400 m at Site 763, where the sediments grade from predominantly calcareous to siliceous-rich material interspersed with dolomitic limestone nodules and beds, suggest that both dolomitization and uptake by clay minerals affect the dissolved Mg profile in this interval.

Unlike Mg, pore-water Ca displays only slight changes with depth. An initial small decrease observed at both sites is consistent with calcite precipitation as proposed to occur in the sediments of Site 765 (Compton, in press). Slight increases in dissolved Ca characterize the rest of the sedimentary sequence at Site 763, whereas a weak negative Ca gradient is observed below 400 mbsf at Site 762. The relatively large increase in the Ca concentration at 404 mbsf (Site 762) is accompanied by a two-fold increase in alkalinity and sharp Mg depletion, and suggests that calcite is dissolving in this interval in addition to reactions that remove Mg from solution. Increases in pore-water Ca at Site 763 between 579 and 930 mbsf, in the sediments of Units V–VII, are primarily associated with terrigenous silica-rich sediments and reactions involving clay minerals.

The Sr profiles mainly reflect the recrystallization of calcite. Extremely strong positive gradients over the first 100 mbsf at both sites are followed by a more subtle increase down to near 400 mbsf at Site 762, whereas a zone of near constant Sr concentration exists between 100 and 350 mbsf at Site 763. The high $\delta Sr/\delta Ca$ ratios ($\sim 100 \times 10^{-4}$) in the carbonates of both sites are indicative of calcite recrystallization (Baker et al., 1982). Dissolved Sr variations below 424 mbsf within lithological Subunit IIIB (Site 762) are likely related to slight changes in lithology in addition to calcite recrystallization.

At Site 763 the zone of recrystallization is well-delineated by a narrow concentration range of 467–500 μmol/L Sr between 90 and 320 mbsf. However, Sr decreases to near 300 μmol/L and remains less than 400 μmol/L in lithological Unit IV in which nannofossil claystones, claystones, and zeolites are first found. Mirror image behavior between Sr and Mg from 600 mbsf to total depth is likely associated with limestone nodule beds (recrystallized calcite and dolomite) within this interval, and suggests that Sr release may accompany Mg uptake during dolomitization.

As in other Leg 122 sites, dissolved Ba is governed by the solubility of $BaSO_4$. Concentrations are generally less than 1 μmol/L unless sulfate concentrations decrease below 7 mmol/L. The first of several large concentration fluctuations at Site 762 occurs at 404 mbsf, where most other constituents also exhibit sharp deviations from their normal trends. Subsequent pore-water Ba increases either coincide with local sulfate minima, or occur where its concentration is below approximately 6 mmol/L. Large crystals of barite were found within the chalks of Subunit IIIB at Site 762 (e.g., Sample 122-762C-42X-6, 110–112 cm) (Haq, von Rad, O'Connell, et al., 1990), attesting to the occurrence of precipitation and dissolution reactions within the sediments. The first of three elevated dissolved Ba concentrations at Site 763 coincides with the alkalinity maximum and sulfate minimum at 319 mbsf. A strong smell of H_2S in cores recovered between 300 and 400 mbsf (Haq, von Rad, O'Connell, et al., 1990) indicates anoxic reducing conditions; the sulfate depletion allows more Ba to dissolve. The abundance of pyrite and centimeter-scale marcasite nodules further attests to the anoxic nature of these sediments. Below 400 mbsf dissolved Ba concentrations decrease but remain significantly higher than observed in sulfate-rich pore water. Pyrite and marcasite also become much rarer below 500 mbsf. Two other Ba maxima farther downhole are not as well delineated nor accompanied by high alkalinities. They do, however, occur in sediments where pyrite is common, thereby indicating the presence of sulfide.

The pore-water Ba spikes were originally discovered when analyzing the glass vial splits (Table 2). Reanalysis of plastic stored splits revealed similar trends, although significantly lower concentrations were found. A comparison of Ba data from the glass and plastic splits is presented in Table 3. Because considerably fewer alkalinity splits were available for reanalysis, the

Table 3. Ba stored in glass vs. plastic.

Core, section, interval (cm)	Depth (mbsf)	Ba[a] (mg/L)	Ba[b] (mg/L)
122-759B-			
3R-3, 145–150	16.9	0.086	0.061
7R-1, 140–150	51.4	0.152	0.065
11R-1, 138–148	89.4	0.204	0.125
14R-1, 140–150	117.9	0.308	0.215
122-760B-			
13R-2, 140–150	352.4	0.240	0.194
16R-3, 140–150	382.4	0.320	0.317
19R-2, 140–150	409.4		0.329
22R-3, 140–150	439.4	0.405	0.393
122-761B-			
1H-2, 145–150	2.9	0.060	0.058
2H-5, 145–150	11.6	0.075	0.049
3H-5, 145–150	21.1	0.060	0.043
4H-5, 145–150	30.6	0.069	0.039
5H-5, 145–150	40.1	0.065	0.059
6H-5, 145–150	49.8	0.050	0.027
7H-5, 145–150	59.1	0.051	0.034
8H-5, 145–150	68.6	0.050	0.044
9H-5, 145–150	78.1	0.053	0.039
10H-5, 145–150	87.6	0.063	0.048
17X-4, 140–150	138.1	0.075	0.063
23X-4, 140–150	195.1	0.080	0.049
30X-2, 140–150	257.1	0.045	0.043
122-762C-			
4X-3, 145–150	193.4	0.618	0.567
10X-4, 145–150	251.9	0.742	0.699
14X-5, 145–150	291.4	0.655	0.699
17X-4, 145–150	318.4	0.910	0.757
20X-2, 145–150	343.9	0.764	0.779
23X-2, 140–150	372.4	1.092	0.975
26X-4, 140–150	403.9	2.381	2.228
32X-2, 140–150	452.9	1.973	2.148
35X-1, 140–150	479.9	3.371	3.289
44X-4, 140–150	569.9	42.23	9.39
50X-2, 140–150	623.9	124.5	9.17
53X-4, 140–150	655.4	18.8	11.8
59X-4, 140–150	712.4	22.6	15.1
62X-4, 140–150	740.9	8.81	6.50
66X-4, 140–150	770.9	60.2	35.4
86X-3, 140–150	886.9	392	30.9
122-763B-			
3X-4, 145–150	205.4	0.890	0.910
9X-4, 145–150	262.4	3.31	3.39
12X-3, 140–150	289.4	85.0	11.1
15X-4, 140–150	319.4	564	215
18X-3, 140–150	346.4	468	66.4
24X-5, 140–150	406.4	303	13.7
27X-4, 140–150	433.4	11.0	7.35
30X-4, 140–150	461.9	41.5	21.5
33X-5, 140–150	491.9	22.8	22.3
36X-4, 140–150	518.9	32.0	35.7

[a] Glass vial splits.
[b] Alkalinity splits stored in plastic.

glass vial data have been used in Figure 3 to delineate trends. These are generally similar but several pore-water Ba maxima observed at Site 762 are not as evident from the alkalinity split analyses. Differences between the two splits are generally greater in samples displaying high Ba concentrations; the reasons for these discrepancies remain unclear.

The profiles shown in Figure 3 reveal extensive sulfate reduction associated with the degradation of organic matter at both Exmouth Plateau sites. Sulfate is nearly 75% depleted within the first 370 mbsf at Site 762. Downhole sulfate concentrations remain low, except for the local maximum of 10.2 mmol/L at 404 mbsf. The sulfate profile suggests that a reaction zone exists below approximately 600 mbsf. At Site 763 sulfate is depleted by more than 50% within the first 150 m of the sediment. A change in slope in the sulfate gradient near 150 mbsf that coincides with lithologic Unit IIA (Haq, von Rad, O'Connell, et al., 1990) likely reflects changes in the diffusion coefficient of the sediments. Based on the sulfate minimum of 1.4 mmol/L at 319 mbsf that corresponds to the alkalinity, Ba, and Ca maxima mentioned above, it is likely that a reaction zone exists near 320 mbsf, a much shallower depth than at Site 762. The variable sulfate profiles in the deeper sections of each site are not a result of analytical error; they likely result from core contamination with seawater because the concentration changes roughly correlate with dissolved Cl and Mg. Overall, sulfate concentrations at both sites are suggestive of diffusion profiles affected by variations in the porosity of the sediments, and suggest that reaction zones exist near the transition from chalks to claystones.

The single-point alkalinity maximum at 404 mbsf at Site 762 that has been previously noted to correspond to significant excursions in the concentrations of many other constituents suggests a zone of calcite dissolution. Above and below this depth alkalinity remains in a range of 2–5 mmol/L. The alkalinity of Site 763 pore water, which is characterized by a broad, well-defined maximum at 320 mbsf, has been discussed in terms of its association with H_2S and sulfate minima, and strongly influences the solubilities of Ba, Fe, and Mn.

The depletion of dissolved K down to approximately 600 mbsf generally correlates with Mg although the two K profiles are more similar than the corresponding Mg profiles. This suggests that different reactions may influence the concentrations of K and Mg in the upper sections of both sites. Below 600 mbsf pore-water K decreases farther within the siliciclastic sediments of both sites and correlates better with dissolved Mg, presumably as a result of ion-exchange reactions with clay minerals. As noted at the Wombat sites, slight dissolved K enrichments over seawater within the first 50 mbsf can most likely be attributed to temperature of squeezing effects (Bischoff et al., 1970).

Dissolved Li concentrations correlate roughly with Sr between 340 and 800 mbsf at Site 762. Gieskes et al. (1983) have reported an association of these elements at Deep Sea Drilling Project (DSDP) Sites 474, 482, and 485, which they attributed to the diagenesis of opaline silica and the associated alteration of volcanic materials. A broad silica maximum that correlates roughly with the Li profile at Site 762 is in agreement with the observations of Gieskes et al. (1983); however, it is unlikely that the alteration of volcanic matter is significant at Site 762 because of the predominance of carbonate and terrigenous sediments in the upper and lower portions of this site, respectively. At Site 763, a notable increase in dissolved Li occurs in the semilithified chalks of Unit II through Unit V. The well-defined Li maximum between 638 and 720 mbsf (in Unit VI and the top of Unit VII) likely represents a reaction zone. Below this depth changes in the dissolved Li concentrations can also be related to silica diagenesis as at many DSDP sites (e.g., Gieskes et al., 1983). The zone of maximum Li concentration, immediately below that where silica concentrations decrease abruptly at Site 763, provides evidence in support of this hypothesis, and may be associated with the conversion of cherts to quartz.

The dissolved silica profiles are remarkably similar throughout Sites 762 and 763 although lithological boundaries between carbonates and siliclastic sediments occur at different depths at each site (Haq, von Rad, O'Connell, et al., 1990).

Because of the large Maestrichtian-Eocene hiatus at Site 763 sediment compositions are substantially different at the two sites below 570 mbsf. More carbonate-rich sediments occur at the former and more siliciclastic/terrigenous sediments abound at the latter. Nonetheless, dissolved silica profiles correlate well with the sedimentary composition. Somewhat elevated concentrations (near 0.47 mmol/L) near the sediment surface coincide with the onset of radiolarian dissolution (e.g., Blome, this volume). Within the first 50 mbsf of both sites radiolarians disappear and dissolved silica decreases to near 0.2 mmol/L. It remains in this range to 150 mbsf and subsequently rises sharply to 0.4–0.8 mmol/L at 200 mbsf. Fluctuations in dissolved silica down to 570 mbsf (Site 762), including a large local maximum (~1.2 mmol/L) at 404 mbsf are likely related to the conversion of amorphous silica to opal-CT. In the lower portions of both sites (600 mbsf total depth), concentrations generally well below 0.5 mmol/L suggest uptake of silica during the formation of quartz, although equilibrium with quartz should lead to much lower concentrations near 0.1 mmol/L. The effect of different lithologies at the two sites appears as a slight upward displacement of the zone in which dissolved silica concentrations drop to less than 0.5 mmol/L at Site 763.

Similarities also exist with the dissolved silica profile at Site 761 although the zone of high reactivity, defined by concentrations between 0.4–1 mmol/L, is compressed over a 200-m interval in the latter. These observations indicate that silica diagenesis is not only dependent on burial depth but is also influenced by both the age and the local lithology of the sediment, in agreement with the findings of Reich and von Rad (1979).

Pore-water salinity decreases at Sites 762 and 763 reflect the depletion of K, Mg, and sulfate down to approximately 500 mbsf. This is substantiated by the relatively constant Cl profiles (Fig. 3) to this depth. Slight decreases in Cl subsequently observed at both sites contribute to the further decrease in salinity down to 800 mbsf. The sharp decrease in salinity and Cl at 850 mbsf at Site 762 occurs at the transition between the calcareous claystones of lithological Unit V and the terrigenous claystones of Unit VI (Haq, von Rad, O'Connell, et al., 1990). At Site 763 the less-pronounced dissolved Cl decrease also coincides with lithological Unit V and the onset of predominantly terrigenous sediments.

Sharp decreases in salinity and Cl can be explained by either the decomposition of gas hydrates or by a lateral input of freshwater (Harrison et al., 1982; Gieskes, 1981; Jenden and Gieskes, 1983). The former can be ruled out because no clathrates were found. It is interesting to note that the low-salinity water (~28 g/kg, Site 762) occurs within the silty-claystone sediments of the Barrow Group equivalent. Because of the predominantly terrigenous nature of these sediments, which extend to the continent, advection of freshwater from Australia is inferred.

Gieskes (1981) proposed that salinities below 31.5 g/kg can be explained by infusion of freshwater at depth in the sediments. Data herein support this hypothesis not only because of the Cl decrease associated with the salinity change, but because the low salinity and Cl zones at both sites correlate (lithologically). Limited freshwater infusion at Site 763 compared to Site 762 may result from the lower porosity at the former. Porosities decrease from 40% at 600 mbsf to 20% at the bottom of Site 763, in the lithologically equivalent interval at Site 762 they range from 40%–50%, whereas the sediments immediately above the low salinity interval have less than 25% porosity (Haq, von Rad, O'Connell, et al., 1990). A low salinity (24 g/kg at 801 mbsf) was also observed near a lithologic boundary in the sediments at Site 765 (Ludden, Gradstein, et al., 1990). At DSDP Site 241 Gieskes (1974) reported the presence of freshwater at least 300 km from shore; similar observations were made at Site 270 in the Ross Sea (Mann and Gieskes, 1975) and at Site 339 on the Vøring Plateau (Gieskes et al., 1978). In most cases the sediments consisted of permeable sandstones that allow substantial flow (Gieskes, 1981). The sediments of Unit VI at Site 762 are nearly twice as permeable as those immediately above, thus restricting diffusion of freshwater into overlying claystones of Unit V.

Although both dissolved Fe and Mn were determined in the surface water samples, these are likely contaminated because they were collected from the ship while on station. Indeed, the measured Mn contents (0.44 and 0.47 μmol/L) are two to three orders of magnitude higher than normal open-ocean water (0.2–3 nmol/L) and at least one order of magnitude greater than observed in continental shelf surface water (Bruland, 1983). The measured concentration of Fe (70 nmol/L) in surface water from Site 763 is also at least an order of magnitude greater than would be expected in open-ocean water; furthermore, Fe concentrations in continental shelf waters are normally extremely low due to its rapid oxidation and removal from seawater (Emerson et al., 1979). Contamination of Fe, possibly from the sampler itself, is also evident in two samples collected with the Barnes "harpoon" (e.g., Table 1, Samples 122-762B-12X-1, 0–10 cm, and 122-762B-18X-1, 0–10 cm), whereas Mn data appear consistent with those from the nearest "squeezed" porewater sample. Because all samples were squeezed using the stainless steel press and no laminar flow hoods were available for "clean sample handling techniques," all Fe concentrations less than 0.5 μmol/L are potentially suspect. Contamination is not as problematic for Mn and a lower limit of reliability is likely for this element.

Low Mn concentrations at Site 763 throughout the range of the alkalinity maximum combined with strong H_2S odors indicate that precipitation of highly insoluble MnS is likely the cause of low dissolved Mn within this interval. This is supported by the large well-defined Mn maximum immediately below this region and which peaks at 492 mbsf. Pore-water Fe profiles are more scattered and exhibit a wider concentration range than those of Mn. A local minimum also occurs at 319 mbsf below which Fe increases to near 10 μmol/L in the interval where high Mn is observed. Another peak in Fe between 700 and 750 mbsf at both sites that is accompanied by a small dissolved Mn increase only at Site 763. Although not well delineated, because of the paucity of pore-water data in the overlying sediments, these correspond to an interval characterized by both pyritized burrows and abundant siderite zones and/or concretions (Haq, von Rad, O'Connell, et al., 1990).

SUMMARY AND CONCLUSIONS

Similarities in pore-water profiles are observed throughout the sediments cored during Leg 122. Paramount among these are large depletions of K, Mg, and sulfate. Another similarity is the generally slight variance of Ca and alkalinity with depth. Within the unconsolidated oozes of all sites, sulfate reduction associated with the bacterial degradation of organic matter should lead to substantial increases in alkalinity. Although local increases are observed at Sites 762 and 763 a slight decrease or no change in alkalinity downhole is more commonly observed. The generally low alkalinities, as well as the absence of large positive Ca gradients that would be expected from the exchange of Mg for Ca in carbonates, indicate that Ca and alkalinity are consumed by reprecipitation of calcite.

Calcite recrystallization in Leg 122 sediments is evidenced by the high pore-water δSr/δCa ratios observed at all sites. The δSr/δCa ratio of Leg 122 carbonates ranges from approximately 35×10^{-4} to 100×10^{-4}. The low values at Sites 760 (34×10^{-4}, 0–70 mbsf) and 761 (46×10^{-4}, 0–230 mbsf) suggest that calcite recrystallization has progressed to a more limited extent at Wombat Plateau sites than at Sites 762 and 763. Higher values at both Sites 762 and 763 (near 100×10^{-4}) attest to extensive recrystallization throughout the thick carbonate sequences. Based on the Sr profiles, recrystallization must begin within the oozes and continue well into the chalks at Sites 762 and 763. Nonetheless, all δSr/δCa ratios observed throughout Leg 122 sites are approximately two- to five-fold greater than the Sr/Ca ratio of $\sim 20 \times 10^{-4}$ found in nannofossil oozes (Baker et al., 1982) and indicate that Sr is excluded during the recrystallization of calcite.

Large depletions of Mg downhole may be attributed partly to the formation of high magnesian calcites and dolomite, although uptake during the formation of smectite also contributes to the observed depletions (Kastner and Gieskes, 1976; Gieskes, 1981, 1985). Hence, carbonate and silicate diagenesis may be intimately related.

The negative K gradients of 1 to 3 mmol/L/100 m observed in Leg 122 sediments are similar to the deep-sea drilling average of 2 mmol/L/100 m noted by Gieskes (1981). However, the usual explanation that K is taken up during the alteration of volcanic matter and underlying igneous rocks seems inappropriate here because relatively little volcanic matter was found in Leg 122 sediments (Haq, von Rad, O'Connell, et al., 1990). Hence other processes such as the formation of K-feldspars in zones of silicification (Gieskes, 1985), or removal of K associated with the uptake of Mg in authigenic clays, must control the dissolved concentration of this element. An association of K uptake with dolomitization is unlikely.

Dissolved silica trends at Sites 761–763 are interpreted to represent (1) early dissolution of radiolarians near the sediment surface, (2) continued dissolution of opal-A, and (3) precipitation of opal-CT. Below the opal-CT region the decrease to 0.4–0.6 mM represents the zone in which conversion of opal-CT to quartz occurs. Large silica fluctuations observed in the opal-CT zone have been described in terms of both variable and high dissolved silica concentrations remaining in sediments after opal-CT precipitation (Gieskes, 1981), and by local lithologic control on the silica solubility. Subsequent decreases in dissolved silica have also been reported to result from uptake by authigenic clays (Kastner and Gieskes, 1976), although a significant amount of the dissolved silica must go into the formation of authigenic quartz.

Lithium enrichments that generally occur immediately below the zone in which porewater silica concentrations decrease to less than 0.5 mM (Fig. 3) are likely due to the exclusion of Li during recrystallization of opal-CT to quartz (Gieskes, 1981).

Early work by Lerman (1975, 1977) and subsequent studies by McDuff and colleagues (e.g., McDuff and Gieskes, 1976; McDuff et al., 1978; McDuff, 1981, 1985) have treated porewater profiles with simple advection/diffusion models. The models imply that nonlinear pore-water gradients are indicative of reaction zones. Without performing the calculations used in their models, the slight curvature of the Ca, K, and Mg profiles in Leg 122 sediments suggests that reaction zones occur within the sediments at Sites 759, 760, 762, and 763. Even when the gradients appear linear, it is only so over limited intervals. Often the changes in gradient (i.e., their slope) correlate to changes in sediment lithology and porosity and arise from different rates of diffusion within the sediments. Hence the profiles may still be primarily diffusion profiles affected by a variable sediment porosity. Profiles of other constituents such as Li, Sr, silica, and sulfate display much more curved gradients, suggesting that these elements are extensively and actively involved in reactions within the sediment column. This is particularly true for silica; it is generally accepted that the high reactivity of this constituent is commonly sufficient to prevent the erasing of large concentrations gradients by diffusion.

In addition to the diffusive control on pore-water profiles, there is evidence of advective transport of freshwater in several Leg 122 sites. It is likely that a continued infusion of freshwater deep within Site 762 and 763 sediments contributes to the maintenance of significant negative Cl and salinity gradients. Such a process likely occurs, although to more a limited extent at the Wombat Plateau sites.

ACKNOWLEDGMENTS

I wish to express my appreciation to shipboard colleagues and to B. Haq, S. O'Connell, and U. von Rad for educating me in the ways of ODP, and providing a collegial working environment. Many thanks to Joe Powers and Matt Mefferd, and to Charles Fraley and Wayne Shibata, for technical assistance at sea and on shore, respectively. Discussions with Mike Mottl and Joris Gieskes helped me understand and interpret the data presented in this paper. Reviews by J. Compton, S. O'Connell, and an anonymous reviewer helped significantly improve the manuscript. The financial research support provided by JOI/USSAC is deeply appreciated. This is SOEST contribution number 2403.

REFERENCES

Baker, P. A., Gieskes, J. M., and Elderfield, H., 1982. Diagenesis of carbonates in deep-sea sediments: evidence from Sr^{2+}/Ca^{2+} ratios and interstitial dissolved Sr^{2+} data. *J. Sediment. Petrol.*, 52:71–82.

Bischoff, J. L., Greer, R. E., and Luistro, A. O. 1970. Composition of interstitial waters of marine sediments: temperature of squeezing effect. *Science,* 167:1245–1246.

Bruland, K. W., 1983. Trace elements in seawater. *In* Riley, J. P., and Chester, R. (Eds.), *Chemical Oceanography* (Vol. 8): London (Academic Press), 157–220.

Couture, R., Miller, R. S., and Gieskes, J. M., 1977. Interstitial water and mineralogical studies, Leg 41. *In* Lancelot, Y., Seibold, E., et al., *Init. Repts. DSDP,* 41: Washington (U.S. Govt. Printing Office), 907–914.

Compton, J. S., in press. Early diagenesis and the origin of diagenetic carbonate in sediment recovered from the Argo Basin, northeastern Indian Ocean (Site 765). *In* Gradstein, F. M., Ludden, J. N., et al., *Proc. ODP, Sci. Results,* 123: College Station, TX (Ocean Drilling Program).

De Carlo, E. H., 1990. Ion-exchange chromatography and ICP/AES determination of lanthanide series elements in marine Fe-Mn deposits. *Sep. Sci. Tech.,* 35:781–798.

Emerson, S., Cranston, R. E., and Liss, P. S., 1979. *Deep Sea Res. Part A,* 26:859.

Exon, N. F., von Rad, U., and von Stackelberg, U., 1982. The geological evolution of the passive margins of the Exmouth Plateau off northwest Australia. *Mar. Geol.,* 47:131–152.

Gieskes, J. M., 1974. Interstitial water studies, Leg 25. *In* Simpson, E.S.W., Schlich, R., et al., *Init. Repts. DSDP,* 25: Washington (U.S. Govt. Printing Office), 361–394.

_______, 1981. Deep-sea drilling interstitial water studies: implications for chemical alteration of the oceanic crust, layers I and II. *In* Warme, J. E., Douglas, R. G., and Winterer, E. L. (Eds.), *The Deep Sea Drilling Project: A Decade of Progress.* Soc. Econ. Paleontol. Mineral. Spec. Publ., 32:149–167.

_______, 1983. The chemistry of interstitial waters of deep-sea sediments: interpretation of Deep-Sea Drilling data. *In* Riley, J. P., and Chester, R. (Eds.), *Chemical Oceanography* (Vol. 8): London (Academic Press), 222–269.

Gieskes, J. M., Elderfield, H., Lawrence, J. R., Johnson, J., Meyers, B., and Campbell, A., 1982. Geochemistry of interstitial waters and sediments, Leg 64, Gulf of California. *In* Curray, J. R., Moore, D. G., et al., *Init. Repts. DSDP,* 64: Washington (U.S. Govt. Printing Office), 675–694.

Gieskes, J. M., Elderfield, H., and Nevsky, B., 1983. Interstitial water studies, Leg 65. *In* Lewis, B.T.R., Robinson, P., et al., *Init. Repts. DSDP,* 65: Washington (U.S. Govt. Printing Office), 441–449.

Gieskes, J. M., Lawrence, J. R., and Galleisky, G., 1978. Interstitial water studies, Leg 38. *Init. Repts. DSDP,* 38 (Suppl.): Washington (U.S. Govt. Printing Office), 121–123.

Gieskes, J. M., Lawrence, J. R., Perry, E. A., Grady, S. J., and Elderfield, H., 1987. Chemistry of interstitial waters and sediments in the Norwegian-Greenland sea, Deep Sea Drilling Project Leg 38. *Chem. Geol.,* 63:143–155.

Gieskes, J. M., and Peretsman, G., 1986. Procedures of interstitial water analysis. *ODP Tech. Note,* 5.

Haq, B. U., von Rad, U., O'Connell, S., et al., 1990. *Proc. ODP, Init. Repts.,* 122: College Station, TX (Ocean Drilling Program).

Harrison, W. E., Hesse, R., and Gieskes, J. M., 1982. Relationship between sedimentary facies and interstitial water chemistry of slope, trench, and Cocos plate sites from the Middle America Trench transect, active margin off Guatemala, Deep Sea Drilling Project Leg 67. *In* Aubouin, J., von Huene, R., et al., *Init. Repts. DSDP,* 67: Washington (U.S. Govt. Printing Office), 603–616.

Jenden, P. D., and Gieskes, J. M., 1983. Chemical and isotopic composition of interstitial water from Deep Sea Drilling Project Sites 533 and 534. *In* Sheridan, R. E., Gradstein, F. M., et al., *Init. Repts. DSDP,* 76: Washington (U.S. Govt. Printing Office), 453–461.

Kastner, M., and Gieskes, J. M., 1976. Interstitial water profiles and sites of diagenetic reactions, Leg 35, DSDP, Bellinghausen Abyssal Plain. *Earth Planet. Sci. Lett.,* 33:11–20.

Kingston, H. M., and Jassie, L. B., 1988. *Introduction to Microwave Sample Preparation:* Am. Chem. Soc.

Lasaga, A. C., and Holland, H. D., 1976. Mathematical aspects of non-steady state diagenesis. *Geochim. Cosmochim. Acta,* 40:257–266.

Lerman, A., 1975. Maintenance of steady state in oceanic sediments. *Am. J. Sci.,* 275:609–635.

_______, 1977. Migrational processes and chemical reactions in interstitial waters. *In* Goldberg, E. D., and McCave, I. N. (Eds.), *The Sea* (Vol. 6): New York (Wiley), 695–738.

Ludden, J. N., Gradstein, F. M., et al., 1990. *Proc. ODP, Init. Repts.,* 123: College Station, TX (Ocean Drilling Program).

Manheim, F. T., and Sayles, F. L., 1974. Composition and origin of interstitial waters of marine sediments based on deep sea drill cores. *In* Goldberg, E. D. (Ed.), *The Sea* (Vol. 5): New York (Wiley), 527–568.

Mann, R., and Gieskes, J. M., 1975. Interstitial water studies, Leg 28. *In* Hayes, D. E., Frakes, L. A., et al., *Init. Repts. DSDP,* 28: Washington (U.S. Govt. Printing Office), 805–814.

McDuff, R. E., 1981. Major cation gradients in DSDP interstitial waters: the role of diffusive exchange between seawater and upper oceanic crust. *Geochim. Cosmochim. Acta,* 45:1705–1713.

_______, 1985. The chemistry of interstitial waters, Deep Sea Drilling Project, Leg 86. *In* Heath, G. R., Burckle, L. H., et al., *Init. Repts. DSDP,* 86: Washington (U.S. Govt. Printing Office), 675–687.

McDuff, R. E., and Gieskes, J. M., 1976. Calcium and magnesium profiles in DSDP interstitial waters: diffusion or reaction? *Earth Planet. Sci. Lett.,* 33:1–10.

McDuff, R. E., Gieskes, J. M., and Lawrence, J. R., 1978. Interstitial water studies, Leg 42A. *In* Hsü, K. J., Montadert, L., et al., *Init. Repts. DSDP,* 42 (Pt. 1): Washington (U.S. Govt. Printing Office), 561–568.

Riech, V., and von Rad, U., 1979. Silica diagenesis in the Atlantic Ocean: diagenetic potential and transformations. *In* Talwani, M., Hay, W., and Ryan, W.B.F. (Eds.), *Deep Drilling Results in the Atlantic Ocean: Continental Margins and Paleoenvironment:* Am. Geophys. Union, Maurice Ewing Ser., 3:315–340.

Schrader, H.-J., 1972. Kieselsaure-Skelette in sedimenten des iberomarok-kanischen Kontinentalrandes und angrendzender Tiefsee Ebenen. *"Meteor" Forschungsergeb. Reihe C,* 8:10–36.

Date of initial receipt: 29 May 1990
Date of acceptance: 2 March 1991
Ms 122B-129